Fundamental Oxidation Processes in the Remote Marine Atmosphere Investigated Using the NO-NO_2-O_3 Photostationary State

Simone T. Andersen[1*], Beth S. Nelson[1], Katie A. Read[1,2], Shalini Punjabi[1,2], Luis Neves[3], Matthew J. Rowlinson[1], James Hopkins[1,2], Tomás Sherwen[1,2], Lisa K. Whalley[2,4], James D. Lee[1,2], and Lucy J. Carpenter[1]

[1]Wolfson Atmospheric Chemistry Laboratories (WACL), Department of Chemistry, University of York, Heslington, York, YO10 5DD, UK.

[2]National Centre for Atmospheric Science (NCAS), University of York, Heslington, York, YO10 5DD, UK.

[3]Instituto Nacional de Meteorologia e Geofísica, São Vicente (INMG), Mindelo, Cabo Verde.

[4]School of Chemistry, University of Leeds, Leeds, LS2 9JT

[*]Corresponding author: simone.andersen@york.ac.uk

1 Abstract

The photostationary state (PSS) equilibrium between NO and NO_2 is reached within minutes in the atmosphere and can be described by the PSS parameter, φ. Deviations from expected values of φ have previously been used to infer missing oxidants in diverse locations, from highly polluted regions to the extremely clean conditions observed in the remote marine boundary layer (MBL), and have been interpreted as missing understanding of fundamental photochemistry. Here, contrary to these previous observations, we observe good agreement between PSS-derived NO_2 ($[NO_2]_{PSS\ ext.}$), calculated from measured NO, O_3, and $j$$NO_2$ and photochemical box model predictions of peroxy radicals (RO_2 and HO_2), and observed NO_2 ($[NO_2]_{Obs.}$) in extremely clean air containing low levels of CO (< 90 ppbV) and VOCs. However, in clean air containing small amounts of aged pollution (CO > 100 ppbV), we observed higher levels of NO_2 than inferred from the PSS, with $[NO_2]_{Obs.}/[NO_2]_{PSS\ ext.}$ of 1.12-1.68 (25^{th}-75^{th} percentile) implying underestimation of RO_2 radicals by 18.5-104 pptV. Potential NO_2 measurement artefacts have to be carefully considered when comparing PSS-derived NO_2 to observed NO_2, but we show that the NO_2 artefact required to explain the deviation would have to be ~ 4 times greater than the maximum calculated from known interferences. If the additional RO_2 radicals inferred from the PSS convert NO to NO_2 with a reaction rate equivalent to that of methyl peroxy radicals (CH_3O_2), then the calculated net ozone production rate (NOPR, ppbV/h) including these additional oxidants is similar to the average change in O_3 observed, within estimated uncertainties, once halogen oxide chemistry is accounted for. This implies that such additional peroxy radicals, cannot be excluded as a missing oxidant in clean marine air containing aged pollution, and that modelled RO_2 concentrations are significantly underestimated under these conditions.

2 Introduction

Tropospheric NO, NO_2 and O_3 are rapidly interconverted during the day via reactions (1-3), where NO is oxidised by O_3 into NO_2, which is then photolyzed into NO and $O(^3P)$, followed by a fast reaction of $O(^3P)$ with O_2 to return O_3.

$$NO + O_3 \rightarrow NO_2 + O_2 \quad (1)$$

$$NO_2 + h\nu \rightarrow NO + O(^3P) \quad (h\nu \leq 410\ nm) \quad (2)$$

$$O(^3P) + O_2 + M \rightarrow O_3 + M \quad (3)$$

The photostationary state (PSS) equilibrium between NO and NO_2 is reached within minutes (Leighton, 1961) if it is not impacted by fresh NO_x emissions and if the photolysis rate does not change quickly such as under rapidly changing cloud coverage (Mannschreck et al., 2004). The photostationary state can be described by the Leighton ratio (Leighton, 1961) (eq. I), where jNO$_2$ is the photolysis rate of NO_2 and φ is the PSS parameter.

$$\varphi = \frac{j\mathrm{NO_2}[\mathrm{NO_2}]}{k_1[\mathrm{NO}][\mathrm{O_3}]} \quad \text{(I)}$$

Under conditions where O_3 is the only oxidant converting NO to NO_2 φ is equal to 1 and NO_2 at PSS can be estimated from the measured NO, O_3, and jNO$_2$ (eq. II).

$$[\mathrm{NO_2}]_{\mathrm{PSS}} = \frac{k_1[\mathrm{NO}][\mathrm{O_3}]}{j\mathrm{NO_2}} \quad \text{(II)}$$

Deviations from φ = 1 suggest the presence of additional chemistry occurring (Calvert and Stockwell, 1983), particularly the conversion of NO to NO_2 by reaction with an oxidant other than O_3, such as hydroperoxy radicals (HO_2) and organic peroxy radicals (RO_2) (reactions 4-5, where R represents any organic functional group) or with halogen oxides (IO, BrO; reactions 6-7) in the marine atmosphere.

$$\mathrm{RO_2} + \mathrm{NO} \rightarrow \mathrm{RO} + \mathrm{NO_2} \quad (4)$$

$$\mathrm{HO_2} + \mathrm{NO} \rightarrow \mathrm{OH} + \mathrm{NO_2} \quad (5)$$

$$\mathrm{IO} + \mathrm{NO} \rightarrow \mathrm{I} + \mathrm{NO_2} \quad (6)$$

$$\mathrm{BrO} + \mathrm{NO} \rightarrow \mathrm{Br} + \mathrm{NO_2} \quad (7)$$

By including these additional NO oxidation reactions, the NO_2 concentration at PSS can be estimated using equation (III). The photostationary state of NO/NO_2 can also be used to estimate the sum of HO_2 and RO_2 (RO_x) or the sum of BrO and IO (XO) in the atmosphere using equation (IV) and (V) and assuming that $k_4 = k_5$ and $k_6 = k_7$, respectively:

$$[\mathrm{NO_2}]_{\mathrm{PSS\ ext.}} = \frac{(k_1[\mathrm{O_3}]+k_4[\mathrm{RO_2}]+k_5[\mathrm{HO_2}]+k_6[\mathrm{IO}]+k_7[\mathrm{BrO}])[\mathrm{NO}]}{j\mathrm{NO_2}} \quad \text{(III)}$$

$$[\mathrm{RO_2}] + [\mathrm{HO_2}] = \frac{j\mathrm{NO_2}[\mathrm{NO_2}]-(k_1[\mathrm{O_3}]+k_6[\mathrm{IO}]+k_7[\mathrm{BrO}])[\mathrm{NO}]}{k_{4,5}[\mathrm{NO}]} \quad \text{(IV)}$$

$$[\mathrm{BrO}] + [\mathrm{IO}] = \frac{j\mathrm{NO_2}[\mathrm{NO_2}]-(k_1[\mathrm{O_3}]+k_4[\mathrm{RO_2}]+k_5[\mathrm{HO_2}])[\mathrm{NO}]}{k_{6,7}[\mathrm{NO}]} \quad \text{(V)}$$

Previous studies reporting deviations in the PSS parameter to estimate RO_x concentrations in the atmosphere are summarised in Table 1, which compares $[RO_x]_{PSS}$ against measured and/or modelled $[RO_x]$. Measurements of RO_x are predominantly conducted using chemical amplification, where each RO_2 and HO_2 molecule in ambient air leads to the formation of several NO_2 molecules by chain reactions caused by the addition of high concentrations of NO and CO (Cantrell et al., 1993b). The resultant NO_2 can be detected and converted back to a RO_x concentration by quantification of the chain length of the reactions via calibration, typically using known concentrations of CH_3O_2 or peroxyacetyl ($CH_3C(O)O_2$) radicals (Cantrell et al., 1993b; Miyazaki et al., 2010; Wood and Charest, 2014). Since the basis of the chemical amplification technique is detection of RO_x radicals from their ability to oxidise NO to NO_2 (reactions 4 and 5), which is also used to estimate RO_x from the PSS, the RO_x concentrations determined from these methods would be expected to agree reasonably well. However, PSS-derived RO_x concentrations are generally higher than both measured values and those calculated from models and steady state equations in rural conditions (Cantrell et al., 1997; Cantrell et al., 1993a; Ma et al., 2017; Mannschreck et al., 2004; Volz-Thomas et al., 2003) with exceptions such as in the Pearl River Delta where PSS-derived and measured RO_x were comparable (Ma et al., 2017). During campaigns in relatively clean regions with moderate influence from pollution (Amazon Basin and Arabian Peninsula), median PSS-derived RO_x/modelled RO_x (both box and 3D) ratios have been shown to be around 1, albeit, with large variations in the data (Tadic et al., 2020; Trebs et al., 2012). In the remote marine boundary layer (MBL), PSS-derived RO_x has been observed to be 1.27 times higher than the measured RO_x over the South Atlantic Ocean, which itself was approximately 4 times higher than box-modelled (Hosaynali Beygi et al., 2011).

Differences between measured, modelled, and PSS-derived RO_x can be due to a variety of reasons. RO_x concentrations calculated by box models rely on comprehensive constraint from co-measured trace gases and a reaction scheme which accurately represents the most important photochemical processes. Incomplete characterization of ambient trace gases and/or reaction schemes can therefore result in uncertain RO_x predictions. Large deviations (factor of ~ 3) between box modelled and measured RO_x levels in a pine forest in the Rocky Mountains were attributed to a combination of a missing photolytic source of HO_2 at midday and a missing reaction forming RO_2 independently of sunlight in the model scheme (Wolfe et al., 2014). PSS-derived RO_x can be significantly over- or underestimated if PSS has not been established, for example due to rapidly changing photolysis rates or local sources of NO_x (Mannschreck et al.,

2004). Another reason for overestimation of PSS-derived RO_x is NO_2 measurement artefacts (Bradshaw et al., 1999; Crawford et al., 1996), which results in overestimated NO_2 concentrations. These are common in chemiluminescence instruments and can be due to photolytic or thermal decomposition of HONO, peroxyacetyl nitrate (PAN), and other nitrate molecules in the atmosphere (Bradshaw et al., 1999; Gao et al., 1994; Parrish et al., 1990; Pollack et al., 2010; Reed et al., 2016; Ridley et al., 1988; Ryerson et al., 2000).

Measurements of RO_x are also not without challenges due to effects from e.g. the high reactivity of RO_x, humidity, non-linearity of the NO_2 detection, and formation of organic nitrates and nitrites. In the first chemical amplification instruments, NO_2 was detected by luminol chemiluminescence, which has a non-linear response to NO_2 resulting in the need for a multipoint calibration (Cantrell et al., 1997). However, more recent instruments use cavity attenuated phase shift (CAPS) spectroscopy (Duncianu et al., 2020; Wood and Charest, 2014), laser induced fluorescence (LIF) (Sadanaga et al., 2004), or cavity ring-down spectroscopy (CRDS) (Liu and Zhang, 2014) for detection of NO_2, all of which have been shown to have a linear response. Chemical amplifiers are usually only calibrated for one or two types of peroxy radicals. However, the chain length of each peroxy radical varies, resulting in a different amount of NO_2 production depending on the mixture of peroxy radicals present, which could lead to over/underestimations depending on the ambient mixture. Additionally, the chain length is significantly affected by humidity due to the increase in HO_2 wall loss on humid surfaces and to an enhanced termination rate of HO_2 by reaction with NO to give HNO_3. HO_2 has been shown to form a complex with H_2O ($HO_2 \cdot H_2O$), which reacts 4-8 times faster with NO, creating HNO_3, at 50% relative humidity (RH) compared to under dry conditions (Butkovskaya et al., 2007; Butkovskaya et al., 2009; Duncianu et al., 2020). This leads to the measured chain length decreasing by a factor of two when going from dry conditions to 40% RH and by a factor of three at 70% RH (Duncianu et al., 2020; Mihele and Hastie, 1998). Finally, the chain length is impacted by the gas reagents (NO and CO). Peroxy radicals and alkoxy radicals (RO) can react with NO to create organic nitrates and nitrites, which terminates the chain reaction, preventing further radical propagation processes. This is favoured by longer chain peroxy radicals, and at high NO concentrations. The formation yield of organic nitrates and nitrites differs from a few percent to up to ~23% depending on the nature of the R group present (Duncianu et al., 2020). The studies summarised in Table 1 using chemical amplification to measure total RO_x have estimated the total uncertainty of the measurements to vary from 10-60% (1σ) with the most recent study estimating the highest uncertainty (Ma et al., 2017).

In the presence of sufficient levels of NO, additional ambient peroxy radicals not accounted for in photochemical models should lead to an underestimation of the simulated production rate of O_3, which occurs via reactions (4) and (5) followed by photolysis of NO_2. The production rate of O_3 ($P(O_3)$) can be calculated using equation (VI):

$$P(O_3) = k_4[NO][RO_2] + k_5[NO][HO_2] \quad \text{(VI)}$$

Volz-Thomas et al. (2003) calculated O_3 production rates from PSS-derived and chemical amplification-measured RO_x during the BERLIOZ campaign in Pabstthum, Germany, resulting in an average of ~ 20 ppbV h^{-1} and ~ 2 ppbV h^{-1} across the campaign, respectively. The large difference was credited to an unknown process that converts NO into NO_2 without causing additional O_3 production (Volz-Thomas et al., 2003). This is possible if NO is oxidised by an oxidant which also destroys O_3, similarly to halogen atoms/halogen oxides. This hypothesis is consistent with observations by Parrish et al. at a mountain station in Colorado, where a missing oxidant of photolytic origin was identified (Parrish et al., 1986). It was shown that if the NO to NO_2 oxidation was completely due to RO_x, the increased O_3 production would result in O_3 levels significantly higher than measured, yet if the oxidant exhibited similar reaction mechanisms to IO, extremely high (70 pptV) mixing ratios of IO would be needed (Parrish et al., 1986). These IO levels are more than an order of magnitude higher than observations in the marine atmosphere (Inamdar et al., 2020; Mahajan et al., 2010; Prados-Roman et al., 2015; Read et al., 2008).

In regions where the net O_3 production rate (NOPR) is negligible or negative during the day due to very low NO levels, it is more relevant to compare the NOPR to the observed change in $[O_3]$. The chemical NOPR can be calculated as the difference between the photochemical processes producing and destroying O_3:

$$NOPR = P(O_3) - L(O_3) \quad \text{(VII)}$$

where $P(O_3)$ is determined using equation (VI) and the loss rate of O_3 ($L(O_3)$), is usually determined from reactions (8-12). Additionally, halogens have previously been shown to cause an O_3 loss of 0.23 ± 0.05 ppbV h^{-1} in the MBL (initiated by reaction 13) (Read et al., 2008), which is in line with other studies suggesting that halogens can have a significant impact on O_3 in marine environments (Saiz-Lopez et al., 2012; Sherwen et al., 2016; Vogt et al., 1999).

$$O_3 + h\nu \rightarrow O(^1D) + O_2 \qquad (\lambda \leq 340 \text{ nm}) \qquad (8)$$

$$O(^1D) + H_2O \rightarrow 2\ OH \quad (9)$$

$$O(^1D) + M \rightarrow O(^3P) \quad (10)$$

$$OH + O_3 \rightarrow HO_2 + O_2 \quad (11)$$

$$HO_2 + O_3 \rightarrow OH + 2\ O_2 \quad (12)$$

$$X + O_3 \rightarrow XO + O_2 \quad (X = Br, Cl, I) \quad (13)$$

The actual rate of change of $[O_3]$ within the planetary boundary layer is also impacted by the physical processes of advection, deposition and entrainment, which complicates comparisons with the NOPR. However, if these physical processes change only negligibly over the course of a day, such as in marine well mixed air masses, their net influence can be deduced from the net night time change in O_3 (Ayers and Galbally, 1995; Ayers et al., 1992; Read et al., 2008), allowing a calculation of the NOPR from observations. A comparison of the observed and calculated NOPR gives an indication of whether production and loss rates of O_3 from known processes are sufficient to explain the observed O_3 tendency (Read et al., 2008).

From the studies shown in Table 1, there is clearly widespread evidence of enhanced PSS-derived RO_2 compared to measurements and models, however, all methods to derive RO_x are not without challenges as described above. The large uncertainties associated with RO_x measurements, especially at high humidities where the chain length is significantly impacted by enhanced wall loss and the production of HNO_3, suggest that measurements could be underestimating RO_x in the atmosphere. Previous studies also find that the additional conversion of NO to NO_2 caused by the extra "RO_2" should only produce minimal additional O_3, or at least lead to additional O_3 destruction, thus inferring an unknown missing oxidant which exhibits different chemical behaviour to peroxy radicals.

Up to 25% of methane removal occurs in the tropical MBL due to the high photochemical activity and humidity resulting in high OH radical concentrations (Bloss et al., 2005). Thus, it is crucially important to understand the fundamental oxidation processes, such as the NO_x-O_3 cycle, occurring in this region. However, remote NO_x measurements are rare due to the difficulty in measuring very low (pptV) mixing ratios. Most previous remote NO_x measurements have taken place during short campaigns and do not give information on seasonal changes and long-term trends (Carsey et al., 1997; Jacob et al., 1996; Peterson and Honrath, 1999; Rhoads et al., 1997). Here, we investigate the photostationary state under clean

marine conditions from three years of observations (2017-2020) at the Cape Verde Atmospheric Observatory (CVAO) in the tropical east Atlantic, representing a unique dataset to investigate NO_x-O_3 chemistry in the remote MBL (Andersen et al., 2021; Carpenter et al., 2010; Lee et al., 2009). We also compare the chemical net O_3 production rate (NOPR) calculated from a box model with NOPR derived from the observed net O_3 rate of change, in order to evaluate the possibility of missing peroxy radicals in this remote environment.

3 Methods

3.1 Measurements

Year-round measurements of meteorological parameters and trace gases including NO, NO_2, and C_2-C_8 VOCs have been conducted at the CVAO (16° 51' N, 24° 52' W) since October 2006. The CVAO is located on the north eastern coast of São Vicente, Cabo Verde. The air sampled predominantly comes from the northeast (see Figure 1) and has travelled over the Atlantic Ocean for multiple days since the last exposure to anthropogenic emissions, with the potential exception of ship emissions (Carpenter et al., 2010; Read et al., 2008). This makes it an ideal location to investigate fundamental photochemistry in an ultra-clean environment.

Wind speed (m/s), wind direction (°), temperature (°C), relative humidity (%), barometric pressure (mbar) and total solar radiation (W/m^2) are measured at a height of 7.5 m using an automatic weather station from Campbell Scientific. NO and NO_2 have been measured using an ultra-high sensitivity NO chemiluminescence instrument, which measures NO_2 by photolytic conversion to NO, at the CVAO since 2006 (Lee et al., 2009). The technique and data analysis have been described in detail elsewhere (Andersen et al., 2021). O_3 is measured using a Thermo Scientific 49i Ozone monitor as described in Read et al. (2008). Photolysis rates of a variety of species were measured in 2020 using a spectral radiometer (a 2-pi sr quartz diffuser coupled to an Ocean Optics QE65000 spectrometer via a 10 m fibre optic cable). Prior to 2020, photolysis rates are calculated in this study based on the correlation between the measured photolysis rates in 2020 and the total solar radiation, as described in the supplementary information. Average $j$$NO_2$ and $j$$O(^1D)$ for different seasons are shown in Table 2. VOCs are measured using a dual channel Agilent 7890A gas chromatograph coupled with a Flame Ionization Detector (GC-FID) and a MARKES Thermal Desorption Unit with an ozone precursor trap that is cooled to -30 °C (Read et al., 2009). Details of the calibration and

uncertainties are given in the World Calibration Centre (WCC)-VOC audit report (Steinbrecher, 2019). Examples of the VOCs measured at the CVAO can be found in Table 2. Carbon monoxide (CO), and methane (CH_4), are measured using a cavity ring-down spectrometer (CRDS), G2401 manufactured by Picarro Inc, following the Global Atmosphere Watch (GAW) recommended technique for long term remote measurements. The instrument is highly linear, has a precision of 1 ppbV and 0.3 ppbV over 10 minutes for CO and CH_4 respectively and no measurable drift (Zellweger et al., 2016; Zellweger et al., 2012).

Time series of NO, NO_2, O_3, jNO_2, $jO(^1D)$, temperature, CO, propene, benzene and CH_4 for July 2017 – June 2020 are shown in figures S4-S6. The specifics of each instrument and their respective measurements can be found in Table 2 and a full description of the CVAO site and associated measurements is given in Carpenter et al. (2010).

3.1.1 NO_2 Measurement Artefact

One of the drawbacks of measuring NO_2 by photolytic conversion to NO is it can be subject to artefacts. These could either be of a photolytic or thermal origin (Bradshaw et al., 1999; Gao et al., 1994; Parrish et al., 1990; Ridley et al., 1988; Ryerson et al., 2000). Photolytic artefacts occur when other compounds containing -NO, $-NO_2$, or $-NO_3$ photolyse to form NO over a similar wavelength range as NO_2 and thereby produce an overestimate of NO_2 in the sample (Pollack et al., 2010). Thermal artefacts are caused by thermally labile compounds which decompose in photolytic converters when they heat up and release NO that is measured by the detector or NO_2 which is immediately photolytically converted to NO and then detected (Reed et al., 2016). Additional artefact can arise from compounds sticking to the converter and creating an artefact when the converter is switched on. The potential NO_2 artefact can be estimated using measured or modelled mixing ratios of a range of potential interfering compounds.

The photolytic contribution can be estimated based on the absorption cross section (ACS) of NO_2 and the potential interferents around the peak wavelength of the diodes used to convert NO_2 into NO (385 ± 5 nm). The ACS of NO_2 and some known interfering compounds over the wavelength range 380-390 nm are shown in Table 3. NO_2 and most of the interferents, with the exception of HONO, show relatively invariant ACSs across these wavelengths. When the ACSs of both NO_2 and the particular interferent are invariant over the spectral output of the

diodes, the ratio at the peak wavelength is used to estimate the potential artefact. However, since the ACS of HONO varies significantly over the range, the HONO/NO_2 ACS ratio has been estimated assuming a Gaussian output of the diodes over the wavelengths. It is also important to take into account whether photolysis of the potential interferent produces NO_2 or NO. If NO is the product, then one converted molecule will be detected as two NO_2 molecules if the conversion efficiency of NO_2 is 50 %. If NO_2 is the product then it will be photolysed to NO with a lower conversion efficiency than NO_2 due to spending less time in the converter than ambient NO_2. However, the conversion efficiency of NO_2 is used here (Table 3) to determine an upper limit of the contribution to the NO_2 artefact. The investigated organic nitrates ($C_2H_5ONO_2$, CH_3ONO_2, *n*- and *i*-$C_3H_7ONO_2$, 1- and 2-$C_4H_9ONO_2$, $CH_3O_2NO_2$, and $CH_3C(O)O_2NO_2$), HNO_3, and NO_3 do not photolyse at 385 nm and have therefore not been included in the evaluation of photolytic artefacts (Atkinson et al., 2004).

The main potential photolytic artefact for the CVAO NO_2 measurements is HONO. Measurements of HONO at the CVAO using a Long Path Absorption Photometer (LOPAP) show levels of up to ~ 5 pptV (Reed et al., 2017), indicating an NO_2 artefact of up to 0.63 pptV. However, these measurements were made using a thermostated inlet system with reactive HONO stripping, where loss of HONO to the sample lines is minimised. The NO_x instrument at the CVAO samples at the end of the glass manifold making it highly likely that a fraction of HONO is lost on the manifold before the air is introduced to the NO_x instrument due to the high surface reactivity of HONO (Pinto et al., 2014; Syomin and Finlayson-Pitts, 2003). Thus, we regard the potential HONO-induced artefact of 0.63 pptV as an upper limit. No other potential photolytic artefacts have been measured at the CVAO, however using the GEOS-Chem model (see section 3.2.2) we calculated seasonal cycles of 20 potential interfering compounds at the CVAO (Figure S7). None of these compounds exhibit major seasonal differences, indicating that any measurement artefact will be fairly constant across the year. The contribution from photolytic degradation of compounds other than HONO is predicted to be less than 0.05 pptV using the estimated conversion efficiency of each compound in Table 3 and the modelled mixing ratios at the CVAO.

Peroxyacetyl nitrate (PAN) is produced in polluted areas and transported to remote regions, where it can thermally decompose into peroxy radicals and NO_2. 5.8% of the available PAN has been shown to thermally decompose in blue light converters (BLC) switched on 40% of the time (Reed et al., 2016). This can cause significant overestimations of NO_2 in colder regions where PAN can build up in the atmosphere due to its long lifetime (Kleindienst, 1994),

however, in warmer regions such as Cabo Verde the overestimation will be substantially lower due to the much shorter lifetime (~ 40-230 minutes at 25°C) (Bridier et al., 1991; Kleindienst, 1994), and hence lower concentration of PAN. At the CVAO, PAN was measured in February 2020 using gas chromatography as described by Whalley et al. (Whalley et al., 2004), however, all measurements were below the limit of detection (LOD) of 6 pptV. We measured the temperature increase of the air within an identical photolytic converter (PLC) to the one used at the CVAO to be less than 1°C in the laboratory, suggesting a minimal shift in the PAN equilibrium in ambient air. We calculate an increase in NO_2 of 0.28 pptV arising from 6 pptV of PAN when increasing the temperature from 298 K to 299 K. Combining photolytic and thermal artefact contributions gives a maximum potential NO_2 artefact of 0.95 pptV at the CVAO, which is within the uncertainty previously reported for the NO_2 measurements (Andersen et al., 2021), as shown in Table 2.

3.2 Modelling

3.2.1 Chemical Box Modelling

A tailored zero-dimensional chemical box model of the lower atmosphere, incorporating a subset of the Master Chemical Mechanism (MCM v3.3.1) (Jenkin et al., 2015) into the AtChem2 modelling toolkit (Sommariva et al., 2020), was used to estimate concentrations of OH, HO_2 and RO_2 and daily chemical production and loss of O_3 at the CVAO. The MCM describes the detailed atmospheric chemical degradation of 143 VOCs, through 17,500 reactions of 6900 species. More details can be found on the MCM website (http://mcm.york.ac.uk, last access: 4th March 2022). A fixed deposition rate of 1.2 x 10^{-5} s^{-1} was applied to all model generated species, giving them a lifetime of approximately 24 hours. The model was constrained to 34 observationally derived photolysis rates, temperature, pressure, and relative humidity, along with a range of observed chemical species, defined in Table 2.

While the box model is constrained to a variety of VOCs, which are expected to be the most dominant at the CVAO, it is only constrained to two oxygenated VOCs (OVOCs); methanol and acetone, due to the lack of reliable measurements of other OVOCs. Acetaldehyde and formaldehyde are expected to be the dominant OVOCs not constrained in the box model. Acetaldehyde from the ATom aircraft campaigns in October 2017, May 2018, and August 2018 show levels of between ~150 and ~250 pptV (Wofsy et al., 2021), which agrees well with

average observations of 180 pptV in the northern hemisphere over the Atlantic Ocean (Yang et al., 2014). Formaldehyde measured at the CVAO in 2006-2007 varied from 350 to 550 pptV (Mahajan et al., 2011). Compared to using the levels generated by the box model of ~8 pptV of acetaldehyde and 270 pptV of formaldehyde, constraining these gases to 150 pptV and 450 pptV, respectively, increases the total RO_x levels by 3% from 52.7 pptV to 54.4 pptV. Thus, we consider that the major VOCs and OVOCs are constrained sufficiently well in the box model for the purpose of simulating HO_2 and RO_2 levels.

3.2.2 GEOS-Chem

Concentrations of 20 different chemical species were extracted every hour during 2019 at nearest point in space and time from the GEOS-Chem model (v12.9.0, DOI:10.5281/zenodo.3950327). The v12.9.0 model as described by Wang et al. (2021) was run at a nested horizontal resolution of 0.25x0.3125 degrees over the region (-32.0 to 15.0 °E, 0.0 to 34.0 °N), with boundary conditions provided by a separate global model run spun up for one year and with acid uptake on dust considered as described by Fairlie et al. (2010) (Fairlie et al., 2010; Wang et al., 2021).

4 Results and Discussion

Monthly diurnal cycles of HO_2, RO_2, and OH were modelled by constraining the box model to the measurements described in Table 2 (except NO_2) using hourly median concentrations for each month from July 2017 – June 2020 where all the trace gas measurements were available. When measured $j\mathrm{O}(^1\mathrm{D})$ was not available, the hourly average from the same month across the other years was used. Calculated photolysis rates based on total solar radiation (see supplementary) were used up to December 2019 for all other photolysis rates than $j\mathrm{O}(^1\mathrm{D})$.

The modelled OH, HO_2 and RO_2 concentrations agree reasonably well with previous measurements from short term field campaigns based at the CVAO and from various cruises in the Atlantic Ocean (see Figure 2). All the previous measurements of RO_x (HO_2 + RO_2) shown in Figure 2 were conducted using the chemical amplifier technique, which is subject to high uncertainties due to the challenges described above. The box modelled RO_2 shows a strong

correlation with the measured jO(^{1}D), but no correlation to CO (pollution tracer) or CH_4, which is expected to be the primary precursor. Daily diurnal cycles of RO_2 and HO_2 for 9 days in August 2017, 12 days in October 2017, and 20 days in January 2018 were modelled to investigate their daily variability (see Figure S8). Seasonal differences can be observed from the daily outputs, but no major day to day changes within a given month.

4.1 Comparison of measured and PSS NO_2 concentrations

Daily midday (12.00-15.00 UTC, local+1) NO_2 mixing ratios were calculated from the Leighton ratio using equation II ($[NO_2]_{PSS}$), the measured NO, O_3, and jNO_2 and $k_1 = 2.07 \times 10^{-12} \times e^{(-1400/T)}$ (Atkinson et al., 2004) for a three-year period (July 2017 – June 2020). Individual uncertainties of $[NO_2]_{PSS}$ were determined to be 4.20 ± 3.74 pptV (1σ) for each day using the 2σ hourly uncertainties for all the used measurements, which is very similar to the uncertainty of hourly measured $[NO_2]$ (Table 2). Figure 3A shows that $[NO_2]_{PSS}$ significantly underestimates the measured NO_2, indicating that additional oxidants are needed to convert NO into NO_2. Daily midday values of $[NO_2]_{PSS\ ext.}$ were calculated using equation III, where a midday average of each modelled monthly diurnal cycle of HO_2 and RO_2 in Figure 2 was used for all days of their respective month together with previous yearly averaged midday measurements of IO (1.4 ± 0.8 pptV, 1σ) and BrO (2.5 ± 1.1 pptV, 1σ) (Mahajan et al., 2010; Read et al., 2008) at the CVAO. RO_2 was assumed to be equivalent to CH_3O_2, making $k_4 = 2.3 \times 10^{-12} \times e^{(360/T)}$, $k_5 = 3.45 \times 10^{-12} \times e^{(270/T)}$, $k_6 = 7.15 \times 10^{-12} \times e^{(300/T)}$, and $k_7 = 8.7 \times 10^{-12} \times e^{(260/T)}$ (Atkinson et al., 2004). Uncertainties for each estimation of $[NO_2]_{PSS\ ext.}$ were determined using the calculated 2σ hourly uncertainties on the measurements and a 20% uncertainty on all rate coefficients. This gives a total average uncertainty of 4.90 ± 4.12 pptV (1σ), excluding any uncertainties in $[HO_2]$ and $[RO_2]$. $[NO_2]_{PSS\ ext.}$ was calculated using a midday average of the modelled monthly $[HO_2]$ and $[RO_2]$ in Figure 2 as well as the modelled daily midday averages from the diurnal cycles in Figure S8 for August 2017, October 2017, and January 2018. A scatter plot of monthly vs daily calculated $[NO_2]_{PSS\ ext.}$ around the 1:1 line (see Figure S9) verifies the use of monthly calculated $[HO_2]$ and $[RO_2]$ for the remaining analyses.

Figure 3B shows that the agreement between measured and predicted NO_2 was improved significantly by including modelled additional oxidants with the slope of the linear fit increasing from 0.48 to 0.71. The coefficient of determination was similar for both plots:

Figure 3A, $r^2 = 0.81$ and Figure 3B, $r^2 = 0.77$. We next investigate whether the mixing ratio of NO influences the ability of the full PSS equation (equation III) to predict NO_2. Daily midday averages of $[NO_2]_{Obs.}/[NO_2]_{PSS\ ext.}$ are plotted as a function of NO in Figure 4. A ratio of 1 would be expected if all relevant reaction mechanisms have been taken into account. The deviations from 1 in the ratio can be observed to increase with decreasing NO mixing ratio during March-December. The dashed lines in Figure 4 visualise the effect of a constant NO_2 artefact of 0.95 pptV (our calculated upper limit) on the $[NO_2]_{Obs.}/[NO_2]_{PSS\ ext.}$ ratio, showing that the artefact, while small, can explain some of this observed trend. However, only a small dependence on the NO mixing ratio is seen for January and February, where enhancements of $[NO_2]_{Obs.}/[NO_2]_{PSS\ ext.}$ above 1 continue out to 10 pptV of NO. At Hohenpeissenberg, Germany, similar trends with increasing NO_2/NO ratio with decreasing NO have been observed, which were partly explained by measurement uncertainty in NO and partly by the PSS not being established after being perturbed by NO_x emissions or variable $j$$NO_2$ (Mannschreck et al., 2004). An opposite trend to that observed here and at Hohenpeissenberg was observed over the South Atlantic Ocean, with increasing deviations in $[NO_2]_{Obs.}/[NO_2]_{PSS\ ext.}$ with increasing NO_2 from 3-20 pptV (Hosaynali Beygi et al., 2011), which was explained by a missing photolytic oxidation process.

4.2 NO_2 Artefact or Missing Oxidant?

Deviations between $[NO_2]_{Obs.}$ and $[NO_2]_{PSS\ ext.}$ are usually attributed to an unaccounted artefact in the NO_2 measurements or a missing oxidant converting NO into NO_2 (Bradshaw et al., 1999; Carpenter et al., 1998; Crawford et al., 1996; Hauglustaine et al., 1999; Hauglustaine et al., 1996; Hosaynali Beygi et al., 2011; Volz-Thomas et al., 2003). As discussed above, we show that below 5 pptV of ambient NO, our calculated maximum NO_2 artefact of 0.95 pptV starts to have an impact on the $[NO_2]_{Obs.}/[NO_2]_{PSS\ ext.}$ ratio, however, it is not enough to explain the enhancements observed, especially in wintertime at the CVAO.

The production of RO_2 and HO_2 radicals is dependent on the abundance of their VOC and CO precursors as well as on photochemical activity. To investigate whether the availability of VOCs, CO or sunlight was related to the discrepancy between $[NO_2]_{Obs.}$ and $[NO_2]_{PSS\ ext.}$, boxplots of the $[NO_2]_{Obs.}/[NO_2]_{PSS\ ext.}$ ratio are plotted as a function of intervals of the mixing ratio of different precursors and $j$$NO_2$ (Figure 5). The high deviations in $[NO_2]_{Obs.}/[NO_2]_{PSS\ ext.}$ can be observed to be associated with higher measured mixing ratios of CO, ethane, and

acetylene. No obvious trend can be observed in the dependence on $j(NO_2)$, contrast to Hosaynali Beygi et al. (2011), who observed increasing deviations in $[NO_2]_{Obs.}/[NO_2]_{PSS\ ext.}$ with increasing $j(NO_2)$. However, it should be noted that midday $j(NO_2)$ at the sub-tropical CVAO shows relatively little seasonal variation. Figure 5 shows that the abundances of ethene and propene, both of which have atmospheric lifetimes of less than 3 days, do not seem to affect the deviation of $[NO_2]_{Obs.}/[NO_2]_{PSS\ ext.}$ from 1. Conversely, high abundances of CO, ethane, and acetylene, which all have atmospheric lifetimes above 6 weeks (Atkinson et al., 2006), are observed to be associated with higher $[NO_2]_{Obs.}/[NO_2]_{PSS\ ext.}$ ratios. This could indicate that long-range transport of pollutants supplies additional peroxy radicals (or other NO to NO_2 oxidants) at the CVAO, which are not predicted from known sources and photochemistry.

To further evaluate the impact of pollution, $[NO_2]_{Obs.}/[NO_2]_{PSS\ ext.}$ was separated into three categories based on CO mixing ratios; CO < 90 ppbV, 90 ppbV < CO < 100 ppbV, and CO > 100 ppbV. The deviations of $[NO_2]_{Obs.}/[NO_2]_{PSS\ ext.}$ from 1 increase with increasing [CO], with 50^{th} (25^{th}-75^{th}) percentiles of 1.10 (0.82 -1.37) for CO < 90 ppbV, 1.20 (0.97-1.54) for 90 ppbV < CO < 100 ppbV, and 1.50 (1.18-1.78) for CO > 100 ppbV. The small deviation from 1, which is within the uncertainty of our measurements (see below), for CO < 90 ppbV is strong evidence that fundamental oxidation process in ultra-clean marine air, where the main precursors of RO_2 and HO_2 are CH_4 and CO giving CH_3O_2 and HO_2, respectively, are well understood.

An NO_2 artefact of 0.7 pptV would reduce the ratio of 1.10 to 1.00 in air masses with CO < 90 ppbV. Since the minimum value of the artefact is 0 pptV (if there was no conversion of interferent compounds to NO or NO_2), and our estimated upper limit is 0.97 pptV, we therefore consider it a reasonable assumption that the average NO_2 artefact of our instrument at the CVAO is 0.7 pptV. We make the simple *a priori* assumption that this applies across all measurements during the period of analyses. Such an artefact is insignificant when considering total NO_x concentrations, however, it has a non-negligible impact when investigating NO_2/NO ratios in this very low NO_x environment.

Subtracting 0.7 pptV from all the NO_2 observations results in median (25^{th}-75^{th} percentiles) ratios of 1.00 (0.76-1.29) for CO < 90 ppbV, 1.14 (0.89-1.47) for 90 ppbV < CO < 100 ppbV, and 1.42 (1.12-1.68) for CO > 100 ppbV (Table 4). A student's t-test was performed to evaluate whether the two categories where CO < 90 ppbV and CO > 100 ppbV were significantly different. A mean and standard deviation of 1.06 and 0.42 for CO < 90 ppbV

and 1.45 and 0.61 for CO < 100 ppbV results in a t-value of 6.59, which makes the two categories statistically different. Distributions of each category are plotted in Figure 6A. When CO is between 90 and 100 ppbV, the distribution of $[NO_2]_{Obs.}/[NO_2]_{PSS\ ext.}$ shows the highest occurrences at ratios of ~1 and ~1.5. When CO > 100 ppbV, it is evident that either additional oxidants are needed to convert NO to NO_2, or an additional NO_2 artefact of the order of 4.4 pptV is present in these air masses. As an artefact of 0.7 pptV has already been subtracted, and measurements of HONO and PAN and modelled mixing ratios of halogen nitrates indicate a fairly stable artefact across the year, 4.4 pptV of additional artefact seems highly unlikely. This leaves the possibility of a missing oxidant when the sampled air is enhanced in CO.

Using equation (IV) and (V), the required RO_x ($RO_2 + HO_2$) and XO (IO + BrO) concentrations needed to reconcile $[NO_2]_{Obs.}$ with $[NO_2]_{PSS\ ext}$ can be estimated using $k_{4,5} = 2.3 \times 10^{-12} \times e^{(360/T)}$ and $k_{6,7} = 8.7 \times 10^{-12} \times e^{(260/T)}$ (Atkinson et al., 2004). Our calculations are based on two scenarios: (1) that the measured [BrO] and [IO] are correct and there is unaccounted for RO_x, or (2) that the modelled $[RO_x]$ is correct and there is more [XO] than measured. Due to the similar rate coefficients for IO and BrO reacting with NO, a combined XO can be estimated. The results are summarised in Table 4 based on the three CO categories. The median required RO_x was determined to be 65.0 (33.68 - 112.5, 25^{th}-75^{th} percentile) pptV and 109.7 (63.14 - 149.5, 25^{th}-75^{th} percentile) pptV for 90 ppbV < CO < 100 ppbV and CO > 100 ppbV, respectively. RO_x measurements during the ALBATROSS cruise varied from 40-80 pptV while in the North Atlantic, however, with a reported uncertainty of 25% (1σ) they could be as high as 100 pptV (Burkert et al., 2001). Such concentrations are comparable to the required median RO_x in this study of 109.7 pptV when CO > 100 ppbV. The uncertainty reported for ALBATROSS is similar to many other studies which have reported 10-36% uncertainty on chemical amplification RO_x measurements (Cantrell et al., 1997; Clemitshaw et al., 1997; Handisides et al., 2003; Hernández et al., 2001; Hosaynali Beygi et al., 2011; Volz-Thomas et al., 2003), however, a recent study in the Pearl River Delta reported an uncertainty of 60% (1σ) (Ma et al., 2017). This combined with measurements up to ~150 pptV of RO_x in the South Atlantic Ocean (Hosaynali Beygi et al., 2011) indicates that our required RO_x levels of ~ 100 pptV may not be unrealistic in the MBL.

The median required RO_x ($[RO_x]_{PSS}$) can be observed to be ~2.5 times higher than the levels estimated using the box model for air masses where CO > 100 ppbV, whereas the required [XO] is a factor of ~6.5 higher than previous observations at the CVAO (Mahajan et al., 2010; Read et al., 2008). Across the three categories, the daily median ratio of

$[RO_x]_{PSS}/[RO_x]_{Model}$ is 1.5, which is similar to those observed in previous studies both in remote and rural regions (see Table 1). The additional XO required to reconcile $[NO_2]_{Obs.}$ with $[NO_2]_{PSS\ ext.}$ was determined for each CO category by subtracting the previous measured average concentration of 3.9 pptV (2.5 pptV BrO + 1.4 pptV IO) (Read et al., 2008) from the required XO. Since CO, the main precursor for HO_2, is constrained by measurements in the model, the calculated $[HO_2]$ is assumed to be correct. Thus, we estimate the required and unaccounted for RO_2 assuming it is all in the form of CH_3O_2 from:

$$[RO_2]_{\text{Required}} = \frac{jNO_2[NO_2]-(k_1[O_3]+k_5[HO_2]+k_6[IO]+k_7[BrO])[NO]}{k_4[NO]} \quad \text{(VIII)}$$

$$[RO_2]_{\text{Unaccounted}} = \frac{jNO_2[NO_2]-(k_1[O_3]+k_5[HO_2]+k_6[IO]+k_7[BrO])[NO]}{k_4[NO]} - [RO_2]_{\text{model}} \quad \text{(IX)}$$

Figures 6B and C, show that the unaccounted for RO_2 or XO level increases with increasing [CO], reaching a median of 61.3 pptV and 22.7 pptV, respectively, for air masses where CO > 100 ppbV, which is approximately 2.2 times the box modelled RO_2 and 5.5 times the measured XO in the same air masses. Such an increase in organic peroxy radicals would, under more polluted conditions, cause a major increase in O_3 production during a day (Volz-Thomas et al., 2003). We next examine the impact of additional RO_2 on the net O_3 production rate in Cabo Verde.

4.3 Chemical O_3 Loss

The daily chemical loss of O_3 between 09.30 (09.00-10.00) and 17.30 (17.00-18.00) UTC was used to evaluate whether the PSS-derived $[RO_2]$ was consistent with the net chemical destruction of O_3 at the CVAO. As discussed above, the measured O_3 mixing ratio in the MBL is affected by loss mechanisms in the form of photolysis, reactions with HO_x and halogens, and deposition, and by production through NO_2 photolysis and by entrainment from the O_3-enriched free troposphere. Due to the very stable meteorological condition of the MBL, the variability in entrainment and deposition between night and day is expected to be negligible (Ayers and Galbally, 1995; Ayers et al., 1992; Read et al., 2008). A combined entrainment/deposition term can therefore be estimated from night time O_3 measurements, when there is no photochemical production or loss. An hourly entrainment/deposition term was determined for each month using the average change in O_3 between 22.30 (22.00-23.00) and 03.30 (03.00-04.00), and found to vary from 0.18 ppbV h^{-1} in January to 0.35 ppbV h^{-1} in May,

514 which is in good agreement with previous measurements at the CVAO of 0.18-0.48 ppbV h^{-1}
515 (Read et al., 2008). The observed daily change in O_3 ($\Delta O_{3\ obs.}$) (09.30-17.30) was determined
516 to be -0.40 ± 0.32 ppbV h^{-1} (1σ) across the three years (2017-2020), which is almost identical
517 to the -0.41 ± 0.33 ppbV h^{-1} (1σ) observed at the CVAO in 2007 (Read et al., 2008), but roughly
518 2 times the daily $\Delta O_{3\ obs.}$ in baseline air at Cape Grim (-0.24 ± 0.32 ppbV h^{-1}, 1σ) and Mace
519 Head (-0.20 ± 0.21 ppbV h^{-1}, 1σ) (Carpenter et al., 1997) and 2-40 times the modelled O_3 loss
520 at Mauna Loa (-0.01 to -0.21 ppbV h^{-1}) (Cantrell et al., 1996; Ridley et al., 1992).

521 By subtracting the monthly average entrainment/deposition term from the observed
522 daily ΔO_3, the daily chemical loss of O_3, $\Delta O_{3\ chem.}$, is obtained. The observations were filtered
523 to exclude periods where the change in CO concentration over the interval period, ΔCO, was
524 outside 1 standard deviation of the mean ΔCO, to avoid the ΔO_3 determination being affected
525 by changing air masses. The resulting observed chemical loss of O_3 is averaged by month and
526 plotted in black in Figure 7. $\Delta O_{3\ chem.}$ can be observed to follow photochemical activity, with
527 the lowest $\Delta O_{3\ chem.}$ in October-February, where the lowest photolysis rates are measured (see
528 supplementary and Table 2) and highest $\Delta O_{3\ chem.}$ in March-May and September. A small
529 decrease in $\Delta O_{3\ chem.}$ in June-August occurred simultaneously to the small drop in photolysis
530 rates in June-August. Overall, $\Delta O_{3\ chem.}$ varied from -0.48 ppbV h^{-1} in January to -0.88 ppbV h^{-1}
531 in May.

532 In order to evaluate whether these observationally-derived chemical loss rates of O_3 are
533 consistent with PSS-derived peroxy radical concentrations, $\Delta O_{3\ chem.}$ was estimated using a
534 chemical box model incorporating the MCM, as described in section 3.2.1. The model was
535 constrained to all the measurements described in Table 2, except NO_2 and O_3, which were left
536 unconstrained. $\Delta O_{3\ chem.}$ was simulated with box modelled [RO_2] and [HO_2], with (blue line in
537 Figure 7) and without (grey in Figure 7) inclusion of the halogen chemistry described in Table
538 S1, allowing an evaluation of the O_3 loss due to halogens, as previously discussed by Read et
539 al. (2008). Simulations were also performed with [CH_3O_2] constrained to the required RO_2,
540 box modelled [HO_2] and including halogen chemistry (orange in Figure 7). In model runs with
541 halogen chemistry, BrO and IO were constrained to previously measured annual averages ±
542 reported uncertainties (blue shaded area in Figure 7) (Read et al., 2008). Diurnal cycles of the
543 required RO_2 were constructed using the median of the daily midday averages for each month
544 determined using equation (VIII) for the peak concentration at midday, 1 pptV overnight and
545 interpolating linearly in between.

Figure 7 shows that all three modelled $\Delta O_{3\ chem.}$ exhibited very similar seasonality as the observed $\Delta O_{3\ chem.}$. The difference between running the box model with and without halogen chemistry was 0.24 ± 0.02 ppbV h^{-1} (1σ), which is almost equivalent to the results of Read et al. (2008) from the CVAO of 0.23 ± 0.05 ppbV h^{-1} (1σ). From May-December, the box modelled $\Delta O_{3\ chem.}$ was almost identical whether using modelled RO_2 or constraining CH_3O_2 to the required RO_2, and both were very similar to observed $\Delta O_{3\ chem.}$. The largest difference in $\Delta O_{3\ chem.}$ between using box modelled RO_2 and constraining CH_3O_2 is observed in January where the difference reached 0.09 ppbV h^{-1}, however, this is caused by constraining CH_3O_2 to 100 pptV, which is 5 times more than the modelled RO_2. The average difference between the observed and box modelled $\Delta O_{3\ chem.}$ is 0.06 ± 0.07 ppbV h^{-1} (1σ) when constraining CH_3O_2 to the required RO_2 and 0.04 ± 0.07 ppbV h^{-1} (1σ) when using box modelled RO_2.

Overall, the very small differences in modelled $\Delta O_{3\ chem.}$ whether including the unaccounted for RO_2 or not are a function of the highly NO_x-limited conditions of the remote MBL, where O_3 production is relatively insensitive to the mixture and abundance of peroxy radicals (Sillman, 1999). Thus, although our analysis shows that peroxy radicals with the equivalent O_3 production potential as CH_3O_2 cannot be ruled out as the missing oxidant in marine air masses with aged pollution, neither does it provide robust evidence that the missing oxidant is O_3-producing. Nevertheless, the deviation between PSS-derived peroxy radicals in this study and previous measurements can potentially be explained by the difficulty in measuring peroxy radicals, as discussed above. This would have important consequences for our understanding of O_3 production under higher NO_x conditions.

5 Conclusions

In the remote MBL (CO < 90 ppbV, NO_x < 43 pptV (90^{th} percentile = 23 pptV)) we have shown that the observed NO_2/NO ratio is consistent with fundamental photochemical theory, and that neither missing oxidants nor deviations of the photostationary state are required to reconcile observations with the calculated NO_2/NO ratio. This is to our knowledge the first time this has been shown in a low NO_x environment. However, observed NO_2 levels became increasingly higher than predicted as the CO mixing ratio increased and the air more influenced by long range transport of air pollution in winter. A detailed analysis of potential NO_2 measurement artefacts at the CVAO showed that such artefacts were unlikely to account for these deviations, thus we evaluated the case for a missing NO to NO_2 oxidant. The required

oxidant in air masses with CO > 100 ppbV reached a median of 109.7 pptV when treated as CH_3O_2. These levels are ~ 2.5 times higher than both our box modelled RO_x ($RO_2 + HO_2$) and previous measurements of RO_x measured by chemical amplification at the CVAO. However, chemical amplification measurements are known to be highly uncertain due to the difficulty in determining the chain length of the mixture of RO_2 in the ambient matrix, and we note that the box modelled O_3 production at the CVAO, with the inclusion of these additional peroxy radicals, did not deviate significantly from the observed O_3 production. Overall, we conclude that there is strong evidence for a missing oxidant in remote marine air impacted by long range transport of pollution, and that peroxy radicals cannot be ruled out as to their identity.

6 Acknowledgements

The authors would like to thank the UK Natural Environment Research Council/ National Centre for Atmospheric Science (NERC/NCAS) through the Atmospheric Measurement and Observation Facility (AMOF) for funding the CVAO programme. STA's PhD was supported by the SPHERES Natural Environment Research Council (NERC) Doctoral Training Partnership (DTP), under grant NE/L002574/1. LJC acknowledges funding from the European Research Council (ERC) under the European Union's Horizon 2020 programme (project O3-SML; grant agreement no. 833290).

7 Author Contributions

Data analysis has been performed by STA. The box model has been run by BSN. Back trajectories have been modelled by MR. GEOS-Chem has been run by TS. The instruments at the CVAO have been run by STA, KAR, SP, JH, and LN. KAR and LKW have processed the spectral radiometer data. The manuscript has been written by STA, LJC, JDL, BSN, and KAR.

8 Additional Information

The authors declare that they have no competing interests.

8.1 Data availability:

NO_x, VOCs, meteorological data, CO and O_3: WDCRG (World Data Centre for Reactive Gases)/Norwegian Institute for Air Research (NILU) EBAS database (EBAS (nilu.no))

CH_4 and CO: WDCGG (World Data Centre for Greenhouse Gases) (kishou.go.jp)

9 Figures

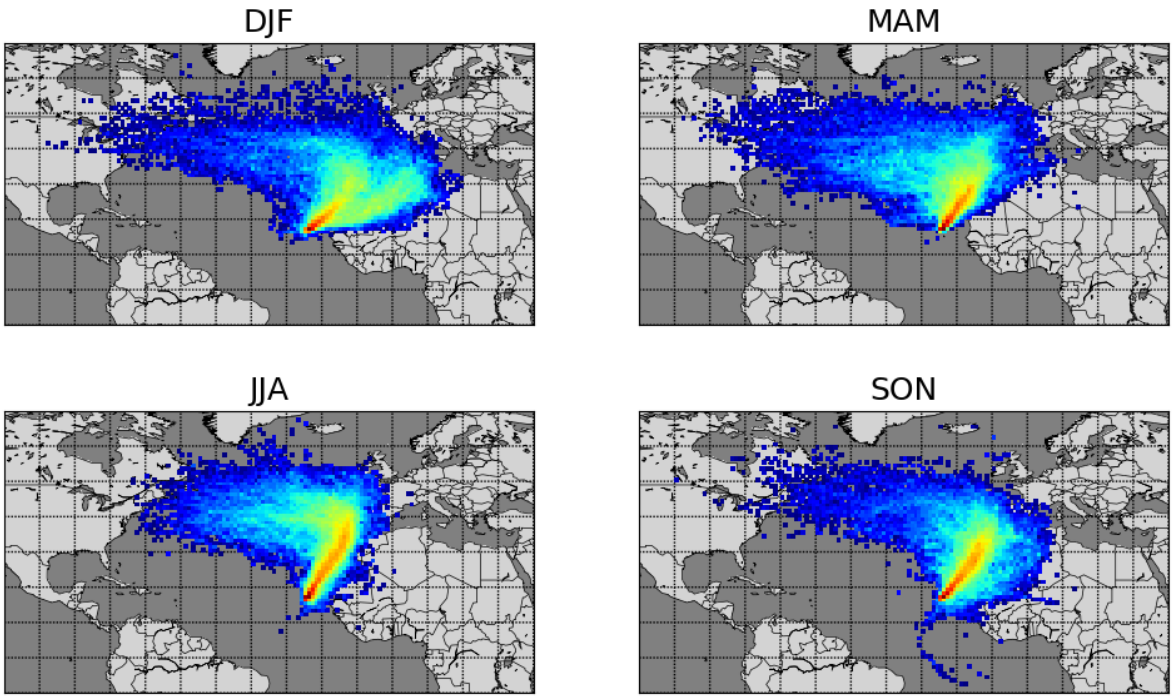

Figure 1: Seasonal average 10-day back trajectories for the CVAO. Locations of released particles are plotted on a 1°x1° grid, determined using FLEXPART as described in Andersen et al. (2021).

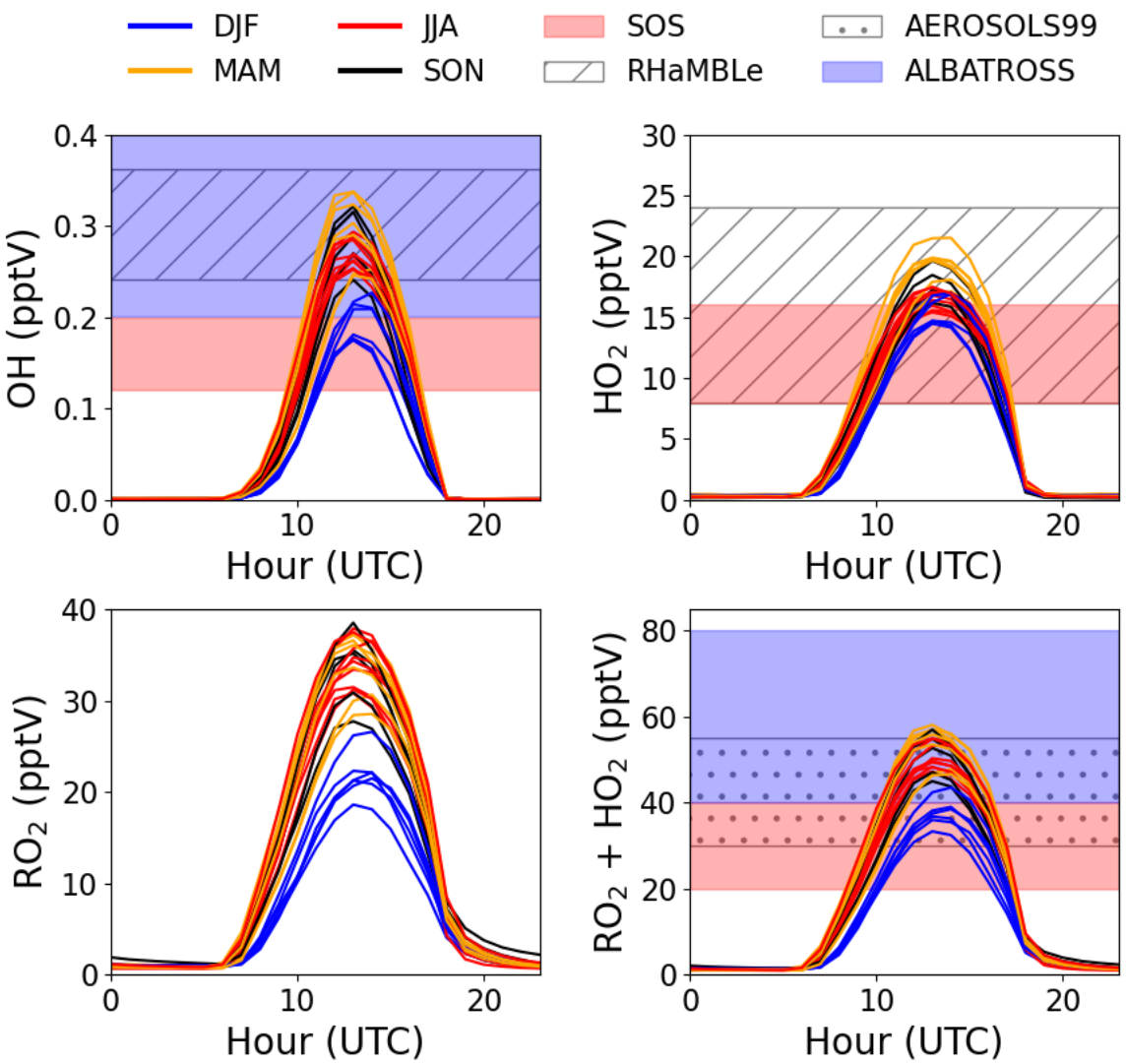

616

617 Figure 2: Average monthly diurnal cycles of modelled OH, HO_2, RO_2, and HO_2+RO_2 coloured
618 by season compared to midday measurements during SOS (February, May, September, and
619 November) (Carpenter et al., 2010; Vaughan et al., 2012), RHaMBLe (May and June) (Whalley
620 et al., 2010), AEROSOLS99 (January and February) (Hernández et al., 2001), and
621 ALBATROSS (November and December) (Burkert et al., 2001).

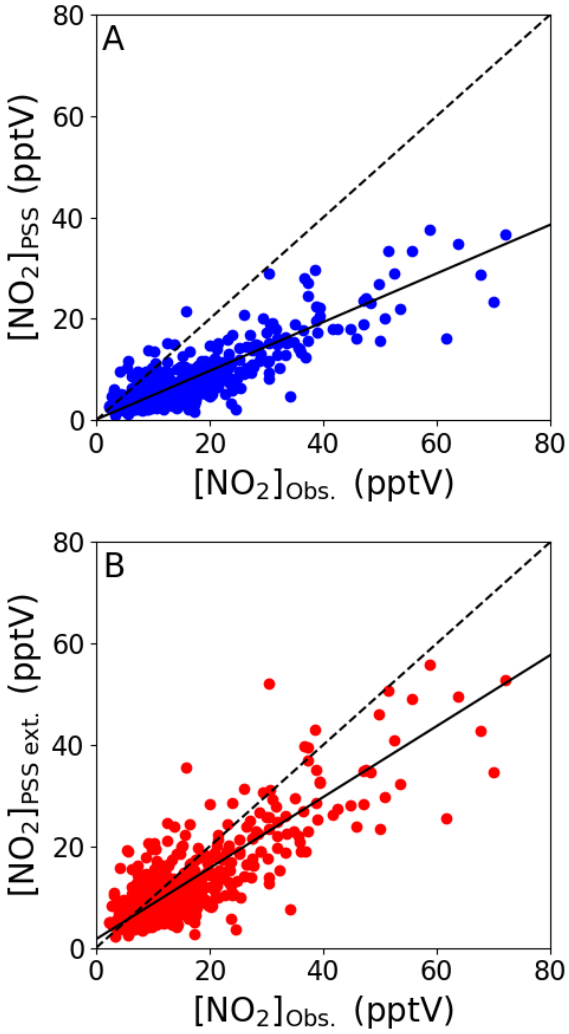

Figure 3: Midday (12.00-15.00 UTC, local+1) daily averages of $[NO_2]_{PSS}$ (A) and $[NO_2]_{PSS\ ext.}$ (B) plotted against the observed NO_2 using measurements from July 2017 – June 2020. The black dashed lines show the 1:1 ratio and the solid black lines show the linear fit to the datapoints (A: $0.48 \times [NO_2]_{Obs.} + 0.16$, B: $0.70 \times [NO_2]_{Obs.} + 1.71$).

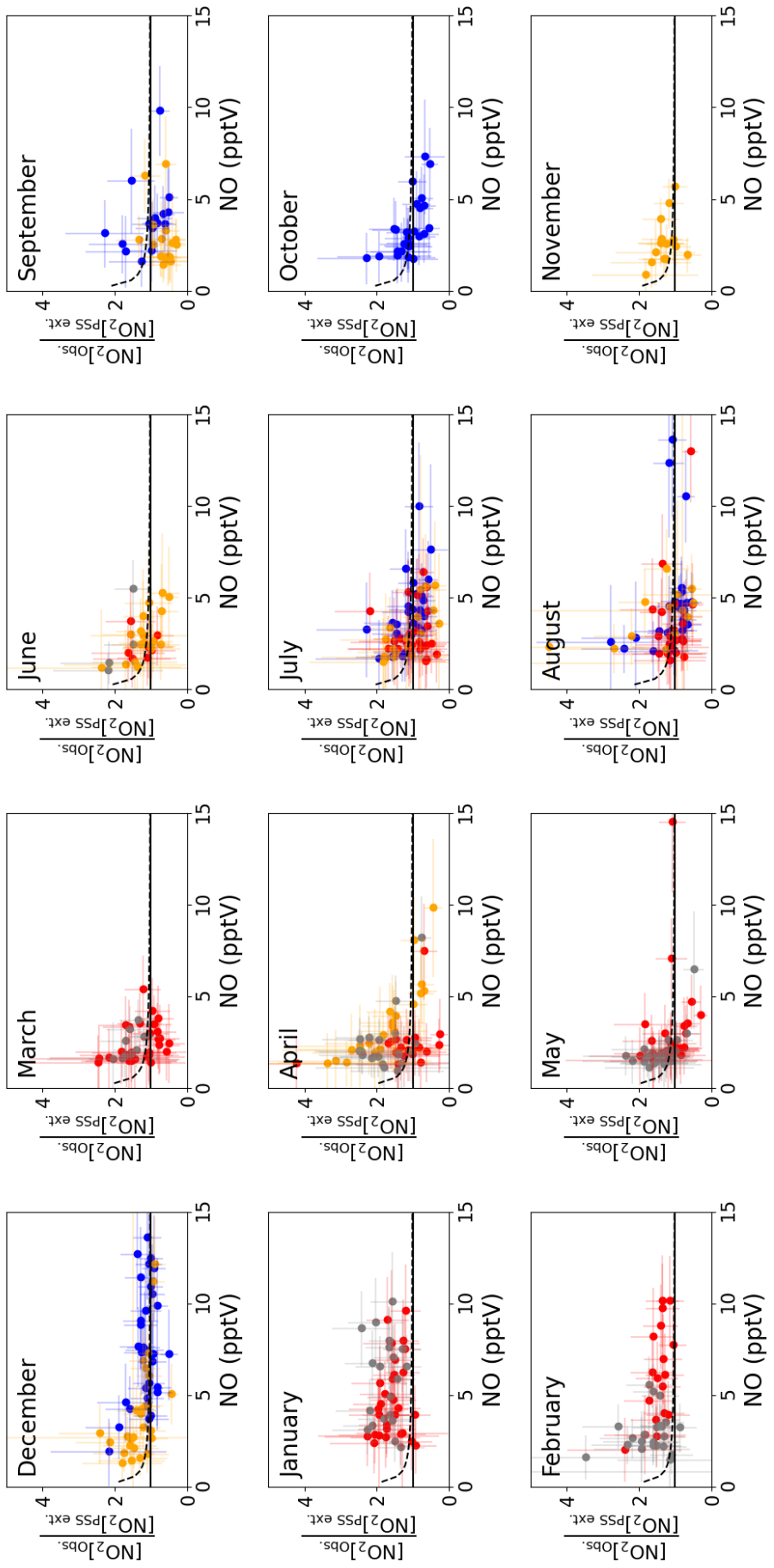
December
January
February
March
April
May
June
July
August
September
October
November
[NO2]Obs. / [NO2]PSS ext.
NO (pptV)
0
2
4
0
5
10
15

627

Figure 4: Monthly plots of midday (12.00-15.00 UTC, local+1) daily averages of $[NO_2]_{Obs.}/[NO_2]_{PSS\ ext.}$ vs. the measured NO mixing ratio. The solid lines represent a ratio of 1 between the observed and predicted NO_2. The error bars represent ± 2σ uncertainty on the calculated ratio and measured NO. The colours represent the year of the measurements: 2017 = blue, 2018 = red, 2019 = orange, 2020 = grey. The dashed lines represent $([NO_2]_{PSS\ ext.}$ + 0.95 pptV)/$[NO_2]_{PSS\ ext.}$ to visualise the effect of a NO_2 artefact of 0.97 pptV on the ratio using the average measured $j$$NO_2$ and O_3 and modelled HO_2 and RO_2 for each month and the annually average measured IO and BrO for the CVAO. The uncertainty of each data point has been determined from measurement uncertainties in Table 2, the uncertainties in the measured BrO and IO described in the text, and 20% uncertainty on all the rate coefficients. The uncertainty in the modelled radicals has not been included

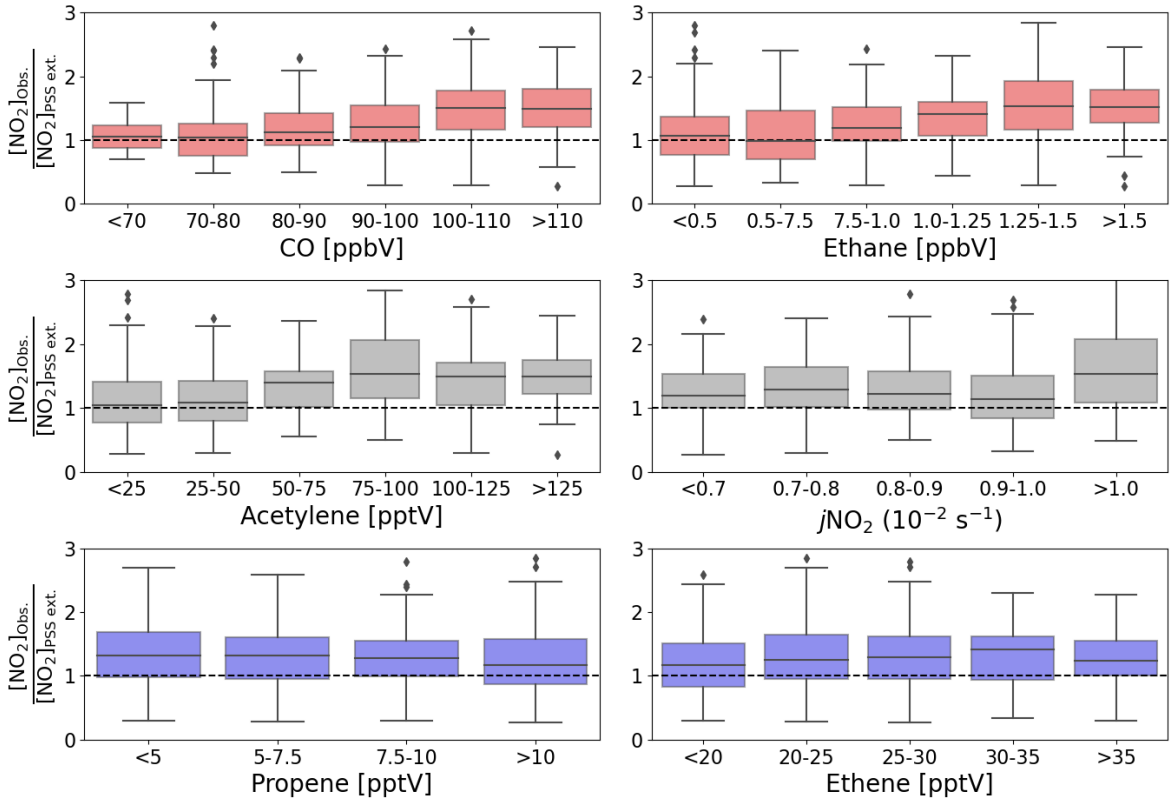

639

640 Figure 5: Boxplots of midday (12.00-15.00 UTC, local +1) daily averages of
641 $[NO_2]_{Obs.}/[NO_2]_{PSS\ ext.}$ from July 2017 to June 2020 plotted against intervals of five different
642 measured precursors for either HO_2 or RO_2 and jNO_2. The black dashed lines represent a ratio
643 of 1.

644

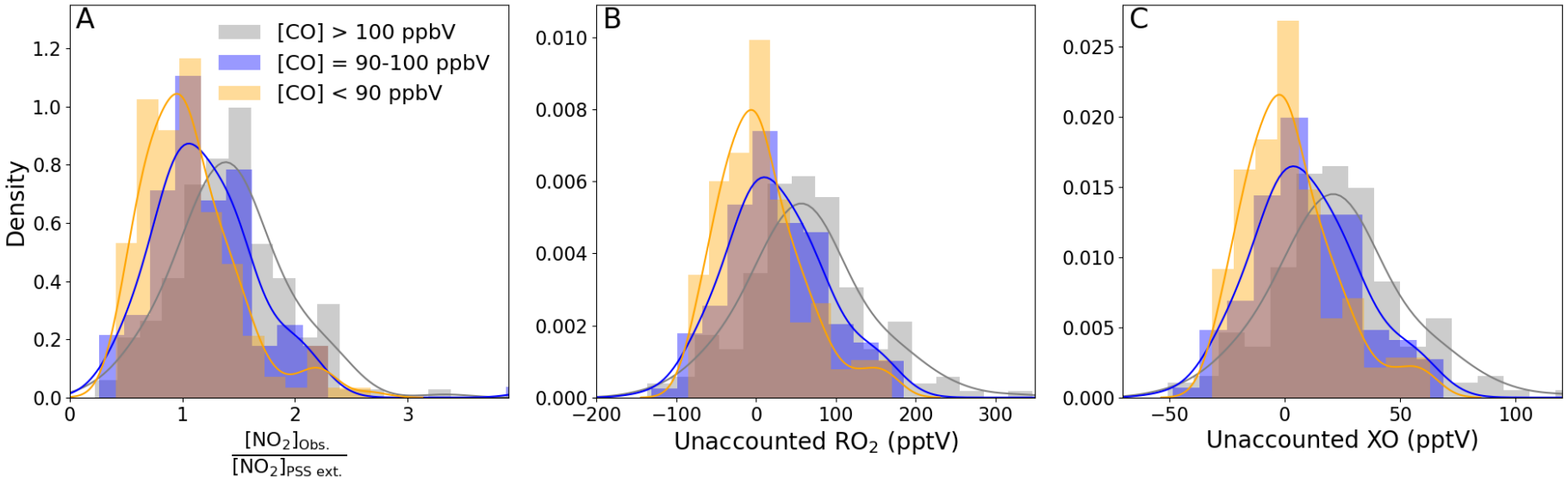
A
[CO] > 100 ppbV
[CO] = 90-100 ppbV
[CO] < 90 ppbV
Density
$\frac{[NO_2]_{Obs.}}{[NO_2]_{PSS\ ext.}}$
B
Unaccounted RO_2 (pptV)
C
Unaccounted XO (pptV)

Figure 6: Density distributions of (A) $[NO_2]_{Obs.}/[NO_2]_{PSS\ ext.}$, (B) missing RO_2, and (C) missing XO separated by measured CO mixing ratios. An NO_2 artefact of 0.7 pptV has been subtracted from all data.

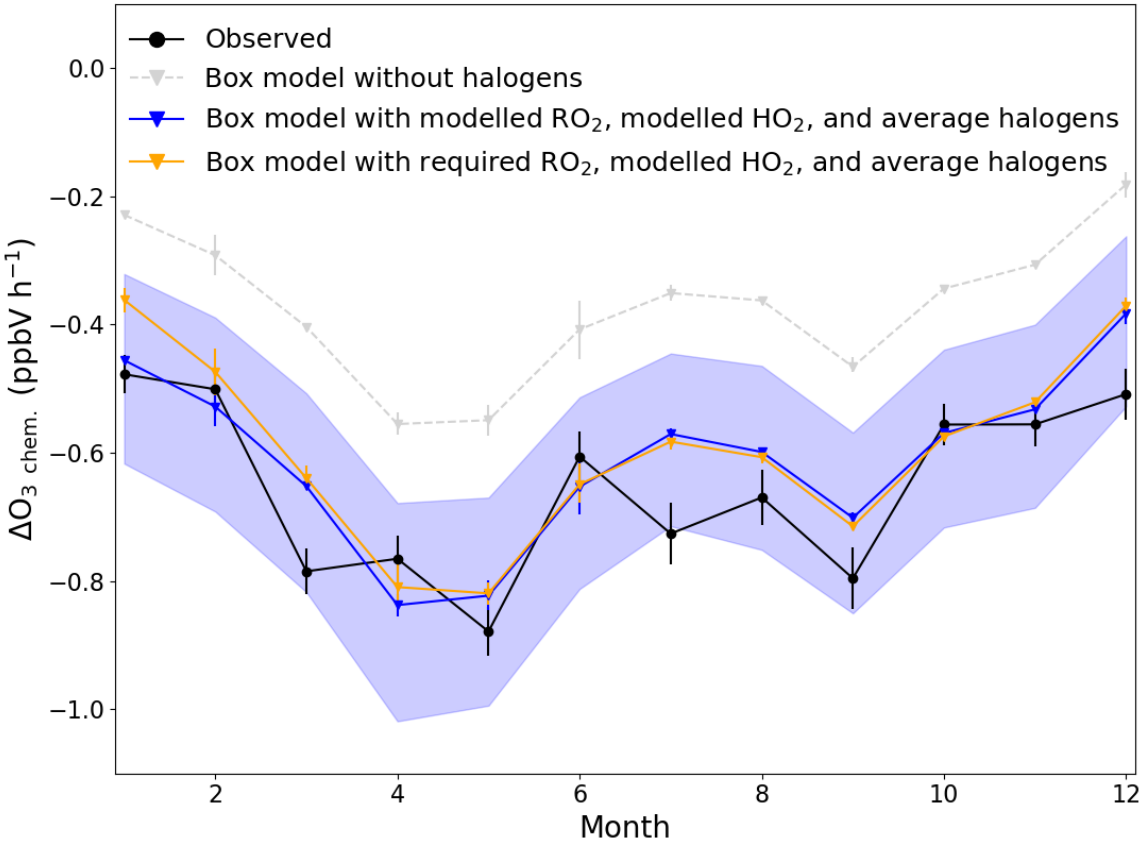

651

652 Figure 7: Average monthly ΔO_3 due to chemical loss between 09.30 (09.00-10.00) and 17.30
653 (17.00-18.00) UTC for each month (black) compared to box modelled ΔO_3 due to chemical
654 loss using modelled RO_2 and HO_2 with (blue) and without (grey) halogen monoxides (BrO and
655 IO), and using required RO_2 to get $[NO_2]_{Obs.}/[NO_2]_{PSS\ ext.} = 1$, modelled HO_2, and the annually
656 averaged halogen monoxides (orange). The error bars on the observed chemical loss is the
657 standard error of all the days used for each month and for the box model it is the minimum and
658 maximum ΔO_3 modelled for each month. The blue shaded area show the possible variability
659 in the chemical loss when including the measured halogens at the CVAO (BrO; 2.5 ± 1.1 pptV,
660 IO; 1.4 ± 0.8 pptV) (Read et al., 2008).

661

10 Tables

Table 1: Summary of previous studies which have compared $[RO_x]_{PSS}$ against measured and/or modelled $[RO_x]$ in rural, marine and remote conditions.

Location	NO_x instrument	NO_x	φ[a]	$\frac{[RO_x]_{PSS}}{[RO_x]_{Measured}}$ [b]	$\frac{[RO_x]_{PSS}}{[RO_x]_{Model}}$ [b]	$\frac{[RO_x]_{Measured}}{[RO_x]_{Model}}$ [b]	Reference
Rural conditions							
Hohenpeissenberg, Germany	CLD with PLC[c]	NO; 50-7000 pptV	2-5.7[d]	2-3[e]	-	-	(Mannschreck et al., 2004)
Pearl River Delta, China	CLD with PLC[c]	NO; 50-4000 pptV	1-8.5[d]	~ 1[e]	2-10	~ 2[e]	(Ma et al., 2017)
Pabstthum, Germany	CLD with PLC[c]	1-7 ppbV	1.1-3.0[d]	~ 4[e]	-	-	(Volz-Thomas et al., 2003)
Idaho Hill, Colorado	CLD with PLC[c]	38 pptV-21.3 ppbV	-	2.1 (mean)[e]	-	~ 1[e, f]	(Cantrell et al., 1997; Williams et al., 1997)
Pine forest, Alabama	CLD with PLC[c]	1-5 ppbV	-	1-2[e]	-	~ 1[e, f]	(Cantrell et al., 1992; Cantrell et al., 1993a; Parrish et al., 1986)
Essex, England	CLD with Mo[g]	NO; 0.3-9.9 ppbV	-	-	-	~ 1.4[e]	(Emmerson et al., 2007)
Ponderosa pine forest, Rocky Mountains	CLD with PLC[c]	NO; 100-150 pptV	-	-	-	<3[h]	(Wolfe et al., 2014)
Marine/Remote with pollution							
Arabian Peninsula	CLD with PLC[c] and CRDS[i]	< 50 pptV - > 10 ppbV	-	-	0.95 (median)	-	(Tadic et al., 2020)
Amazon Basin (Manaus)	CLD with PLC[c]	100 pptV - 30 ppbV	1-6[d]	-	~ 1[k]	-	(Trebs et al., 2012)
Marine/Remote conditions							
South Atlantic Ocean	CLD with PLC[c]	NO_2; 3-20 pptV	1-12.5[l]	1.27[e]	~ 5	~ 4[e]	(Hosaynali Beygi et al., 2011)
Mauna Loa, Hawaii	CLD with PLC[c]	20-60 pptV	1.4-2.2	1.5-3[e]	2-3.5	1.2-2[e]	(Hauglustaine et al., 1996)
Mace Head, Ireland	CLD with TC[m]	NO < 10 pptV	-	-	-	~ 0.25[e]	(Carpenter et al., 1997; Cox, 1999)
Cape Grim, Tasmania	CLD with PLC[c]	NO < 5 pptV	-	-	-	~ 0.4[e]	(Carpenter et al., 1997; Cox, 1999)
Cabo Verde	CLD with PLC[c]	< 50 pptV	0.45-12.0[d] (median = 2.1)	-	1.5 (median)	-	This study

[a]Without radicals and halogens. [b][RO_x] = [HO_2] + [RO_2]. [c]CLD with PLC = Detection by chemiluminescence with photolytic converter for NO_2. [d]Increasing φ with decreasing [NO], [NO_2] or [NO_x]. [e][RO_x] measured by chemical amplification. [f]Calculated/modelled using stead state theory. [g]CLD with Mo = Detection by chemiluminescence with molybdenum converter. [h][RO_x] measured by Peroxy Radical Chemical Ionization Mass Spectrometry (PeRCIMS). [i]CRDS = Cavity Ring down spectroscopy. [k]PSS derived [RO_x] was within the range of the modelled values. [l]Increasing φ with increasing [NO_2]. [m]CLD with TC = Detection by chemiluminescence with thermal converter.

Table 2: Overview of instruments and measurements used from the CVAO.

Instrument	Measurement	2σ Hourly Uncertainty	DJF[a]	MAM[a]	JJA[a]	SON[a]	Reference[b]
AQD	NO (pptV)	1.4 pptV[c] (55 %)[d]	5.3 ± 7.8	1.9 ± 4.2	2.7 ± 5.6	3.6 ± 5.9	Andersen et al. (2021)
	NO_2 (pptV)	4.4 pptV[c] (36 %)[d]	27.0 ± 35.8	10.0 ± 13.5	10.2 ± 16.8	10.6 ± 15.7	
Thermo Scientific 49i	O_3 (ppbV)	0.07 ppbV[e] (< 1 %)	38.9 ± 8.8	39.2 ± 12.1	29.9 ± 11.9	31.2 ± 11.1	Read et al. (2008)
Ocean Optics QE650000	jNO_2 (10^{-3} s^{-1})	15 %	7.8 ± 2.7	9.3 ± 2.2	8.9 ± 2.5	8.7 ± 2.4	See supplementary
	$jO(^1D)$ (10^{-5} s^{-1})	15 %	1.7 ± 1.2	3.0 ± 1.3	2.6 ± 1.2	2.6 ± 1.2	
Picarro	CO (ppbV)	1.0 ppbV (< 2 %)	99.0 ± 20.2	103 ± 17	80.0 ± 19.3	84.5 ± 16.6	Zellweger et al. (2012, 2016)
	CH_4 (ppbV)	0.3 ppbV (< 0.1 %)	1916 ± 26	1914 ± 29	1886 ± 34	1896 ± 30	
GC-FID	Ethane (pptV)	5.2 %	1438 ± 600	1204 ± 608	518 ± 267	660 ± 449	R. Steinbrecher (2019)
	Ethene (pptV)	5.0 %	31.2 ± 18.6	23.2 ± 9.8	27.5 ± 15.1	28.9 ± 19.6	
	Acetylene (pptV)	10.7 %	134 ± 86	86.9 ± 82.4	22.6 ± 22.2	38.1 ± 38.5	
	Propane (pptV)	5.6 %	336 ± 259	148 ± 195	20.6 ± 18.7	71.0 ± 133	
	Propene (pptV)	6.9 %	8.6 ± 8.6	8.8 ± 11.5	8.0 ± 6.2	7.2 ± 6.1	
	Iso-butane (pptV)	6.4 %	40.4 ± 39.5	11.0 ± 20.0	3.2 ± 4.3	8.4 ± 15.5	
	n-butane (pptV)	5.0 %	82.8 ± 80.7	19.4 ± 36.0	6.0 ± 7.3	22.1 ± 40.5	
	Iso-pentane (pptV)	4.6 %	11.1 ± 14.9	3.6 ± 6.2	5.2 ± 9.5	4.0 ± 6.7	
	n-pentane (pptV)	6.4 %	8.7 ± 11.4	2.9 ± 4.7	1.7 ± 2.6	3.5 ± 5.2	
	Benzene (pptV)	4.8 %	40.1 ± 30.5	22.9 ± 23.3	11.1 ± 10.5	17.3 ± 11.5	
	Toluene (pptV)	6.3 %	4.6 ± 5.4	3.0 ± 4.2	2.9 ± 2.8	3.4 ± 3.1	
	Methanol (pptV)	20.7 %	486 ± 563	698 ± 734	677 ± 603	857 ± 655	
	Acetone (pptV)	12.2 %	506 ± 263	614 ± 274	767 ± 332	681 ± 213	
Campbell Scientific weather station	Temperature (°C)	0.4 °C at 5-40 °C	22.0 ± 2.3	21.7 ± 1.4	24.5 ± 2.5	25.8 ± 2.1	Carpenter et al. (2010)
	Pressure (hPa)	1.0 hPa at 0-40°C	1016 ± 4	1016 ± 3	1015 ± 4	1014 ± 3	
	Relative Humidity (%)	2 % at 10-90 %	74.9 ± 12.8	77.2 ± 10.4	82.8 ± 8.8	81.1 ± 11.9	
	Solar Radiation (W m^{-2})	5%	615 ± 312	785 ± 251	737 ± 283	716 ± 273	

[a]Midday (12.00-15.00 UTC, local +1) mean ± 2σ for July 2017 – June 2020. [b]For further information on the instrument and the data processing. [c]Average uncertainties determined as described in Andersen et al. (2021). [d]Percentage given is relevant to average midday uncertainty. [e]Estimated from zero measurements and from running two O_3 instruments together.

Table 3: Potential sources of NO_2 artefacts at the CVAO.

	ACS at 380 nm (10^{-20} cm^2)[a]	ACS at 385 nm (10^{-20} cm^2)[a]	ACS at 390 nm (10^{-20} cm^2)[a]	Conversion efficiency (%)[b]	Measured at the CVAO at midday (pptV)[c]	Modelled by GEOS Chem at midday (pptV)[c]	Potential artefact (pptV)
$NO_2 \xrightarrow{h\nu} NO$	59.24	59.42	62.0	50	-	-	-
$BrONO_2 \xrightarrow{h\nu} NO_2$	3.85	3.37	2.97	2.8	-	0.5-1.5	0.014-0.042
$ClONO_2 \xrightarrow{h\nu} NO_2$	0.121	0.137	0.091	0.1	-	0.5-1	0.0005-0.001
$ClNO \xrightarrow{h\nu} NO$	8.86	7.82	6.86	6.6	-	-	-
$ClNO_2 \xrightarrow{h\nu} NO_2$	0.3593	0.2687	0.2008	0.2	-	~0	-
$BrNO_2 \xrightarrow{h\nu} NO_2$	17	17	16	14.3	-	~0	-
$HONO \xrightarrow{h\nu} NO$	9.2	14.5	2.4	6.3	3-5	0.2-0.4	0.38-0.63
$PAN \xrightarrow{\Delta} NO_2$	-	-	-	~5	< 6	~20	< 0.28
Total	-	-	-	-	-	-	**0.67-0.95**

[a]All absorption cross sections have been reported by IUPAC (Atkinson et al., 2004). [b]The reported conversion efficiencies have been calculated based on a NO_2 CE of 50%. [c]Midday is defined as 12.00-15.00 UTC (local+1).

Table 4: Summary over the required additional artefact, RO_2, and XO to give $[NO_2]_{Obs.}/[NO_2]_{PSS\ ext.}$ = 1 given as 50th (25th-75th) percentile when subtracting a NO_2 artefact of 0.7 pptV.

	[CO] < 90 ppbV	90 ppbV < [CO] < 100 ppbV	[CO] > 100 ppbV
$\frac{[NO_2]_{Obs.}}{[NO_2]_{PSS\ ext.}}$	1.00 (0.76 - 1.29)	1.14 (0.89 - 1.47)	1.42 (1.12 - 1.68)
Required additional artefact (pptV)	0.00 (-2.65 - 1.70)	1.9 (0.92 - 5.27)	4.4 (0.95 - 9.27)
Case I: Using BrO = 2.5 pptV and IO = 1.4 pptV			
Required RO_x (pptV)[a]	49.45 (16.18 - 87.63)	65.0 (33.68 - 112.5)	109.7 (63.14 - 149.5)
Modelled RO_x (pptV)	48.89 (46.01 - 53.35)	45.60 (35.69 - 54.71)	44.99 (37.31 - 54.70)
Required RO_2 (pptV)[b]	31.77 (-1.79 - 69.99)	47.53 (16.81 - 93.93)	90.49 (45.04 - 128.5)
Modelled RO_2 (pptV)	33.66 (30.07 - 34.43)	29.89 (21.50 - 36.32)	27.62 (20.93 - 35.42)
Missing RO_2 (pptV)[c]	-0.25 (-31.85 - 39.69)	20.19 (-14.23 - 66.44)	61.33 (18.53 - 104.3)
Case II: Using modelled RO_2 and HO_2			
Required XO (pptV)[d]	3.72 (-7.94 - 18.55)	11.31 (-1.46 - 28.46)	26.58 (10.70 - 42.52)
Missing XO (pptV)[e]	-0.18 (-11.84 - 14.65)	7.41 (-5.36 - 24.56)	22.68 (6.80 - 38.62)

[a]Calculated using equation (IV). [b]Calculated using equation (VIII). [c]Calculated using equation (IX). [d]Calculated using equation (V). [e]Subtracted 3.9 pptV of XO from the required XO (2.5 pptV BrO + 1.4 pptV IO).

11 References

Andersen, S. T., Carpenter, L. J., Nelson, B. S., Neves, L., Read, K. A., Reed, C., Ward, M., Rowlinson, M. J., and Lee, J. D.: Long-term NO_x measurements in the remote marine tropical troposphere, Atmos. Meas. Tech., 14, 3071-3085, 10.5194/amt-14-3071-2021, 2021.

Atkinson, R., Baulch, D. L., Cox, R. A., Crowley, J. N., Hampson, R. F., Hynes, R. G., Jenkin, M. E., Rossi, M. J., and Troe, J.: IUPAC Task Group on Atmospheric Chemical Kinetic Data Evaluation, Atmos. Chem. Phys., 4, 2004.

Atkinson, R., Baulch, D. L., Cox, R. A., Crowley, J. N., Hampson, R. F., Hynes, R. G., Jenkin, M. E., Rossi, M. J., Troe, J., and Subcommittee, I.: Evaluated kinetic and photochemical data for atmospheric chemistry: Volume II; gas phase reactions of organic species, Atmos. Chem. Phys., 6, 3625-4055, 10.5194/acp-6-3625-2006, 2006.

Ayers, G. P., Penkett, S. A., Gillett, R. W., Bandy, B., Galbally, I. E., Meyer, C. P., Elsworth, C. M., Bentley, S. T., and Forgan, B. W.: Evidence for photochemical control of ozone concentrations in unpolluted marine air, Nature, 360, 446-449, 10.1038/360446a0, 1992.

Ayers, G. P., and Galbally, I. E.: A preliminary investigation of a boundary layer-free troposphere entrainment velocity at Cape Grim, Baseline 92, 1995.

Bloss, W. J., Evans, M. J., Lee, J. D., Sommariva, R., Heard, D. E., and Pilling, M. J.: The oxidative capacity of the troposphere: Coupling of field measurements of OH and a global chemistry transport model, Faraday Discussions, 130, 425-436, 10.1039/B419090D, 2005.

Bradshaw, J., Davis, D., Crawford, J., Chen, G., Shetter, R., Müller, M., Gregory, G., Sachse, G., Blake, D., Heikes, B., Singh, H., Mastromarino, J., and Sandholm, S.: Photofragmentation two-photon laser-induced fluorescence detection of NO_2 and NO: Comparison of measurements with model results based on airborne observations during PEM-Tropics A, Geophysical Research Letters, 26, 471-474, https://doi.org/10.1029/1999GL900015, 1999.

Bridier, I., Caralp, F., Loirat, H., Lesclaux, R., Veyret, B., Becker, K. H., Reimer, A., and Zabel, F.: Kinetic and theoretical studies of the reactions acetylperoxy + nitrogen dioxide + M ⇄ acetyl peroxynitrate + M between 248 and 393 K and between 30 and 760 torr, The Journal of Physical Chemistry, 95, 3594-3600, 10.1021/j100162a031, 1991.

Burkert, J., Andrés-Hernández, M.-D., Stöbener, D., Burrows, J. P., Weissenmayer, M., and Kraus, A.: Peroxy radical and related trace gas measurements in the boundary layer above the Atlantic Ocean, Journal of Geophysical Research: Atmospheres, 106, 5457-5477, https://doi.org/10.1029/2000JD900613, 2001.

Butkovskaya, N., Kukui, A., and Le Bras, G.: HNO3 Forming Channel of the HO_2 + NO Reaction as a Function of Pressure and Temperature in the Ranges of 72−600 Torr and 223−323 K, The Journal of Physical Chemistry A, 111, 9047-9053, 10.1021/jp074117m, 2007.

Butkovskaya, N., Rayez, M.-T., Rayez, J.-C., Kukui, A., and Le Bras, G.: Water Vapor Effect on the HNO3 Yield in the HO_2 + NO Reaction: Experimental and Theoretical Evidence, The Journal of Physical Chemistry A, 113, 11327-11342, 10.1021/jp811428p, 2009.

Calvert, J. G., and Stockwell, W. R.: Deviations from the O_3–NO–NO_2 photostationary state in tropospheric chemistry, Canadian Journal of Chemistry, 61, 983-992, 10.1139/v83-174, 1983.

Cantrell, C. A., Lind, J. A., Shetter, R. E., Calvert, J. G., Goldan, P. D., Kuster, W., Fehsenfeld, F. C., Montzka, S. A., Parrish, D. D., Williams, E. J., Buhr, M. P., Westberg, H. H., Allwine, G., and Martin, R.: Peroxy radicals in the ROSE experiment: Measurement and theory, Journal of Geophysical Research: Atmospheres, 97, 20671-20686, https://doi.org/10.1029/92JD01727, 1992.

Cantrell, C. A., Shetter, R. E., Calvert, J. G., Parrish, D. D., Fehsenfeld, F. C., Goldan, P. D., Kuster, W., Williams, E. J., Westberg, H. H., Allwine, G., and Martin, R.: Peroxy radicals as measured in ROSE and estimated from photostationary state deviations, Journal of Geophysical Research: Atmospheres, 98, 18355-18366, https://doi.org/10.1029/93JD01794, 1993a.

Cantrell, C. A., Shetter, R. E., Lind, J. A., McDaniel, A. H., Calvert, J. G., Parrish, D. D., Fehsenfeld, F. C., Buhr, M. P., and Trainer, M.: An improved chemical amplifier technique for peroxy radical measurements, Journal of Geophysical Research: Atmospheres, 98, 2897-2909, https://doi.org/10.1029/92JD02842, 1993b.

Cantrell, C. A., Shetter, R. E., Gilpin, T. M., and Calvert, J. G.: Peroxy radicals measured during Mauna Loa Observatory Photochemistry Experiment 2: The data and first analysis, Journal of Geophysical Research: Atmospheres, 101, 14643-14652, https://doi.org/10.1029/95JD01698, 1996.

Cantrell, C. A., Shetter, R. E., Calvert, J. G., Eisele, F. L., Williams, E., Baumann, K., Brune, W. H., Stevens, P. S., and Mather, J. H.: Peroxy radicals from photostationary state deviations and steady state calculations during the Tropospheric OH Photochemistry Experiment at Idaho Hill, Colorado, 1993, Journal of Geophysical Research: Atmospheres, 102, 6369-6378, https://doi.org/10.1029/96JD01703, 1997.

Carpenter, L. J., Monks, P. S., Bandy, B. J., Penkett, S. A., Galbally, I. E., and Meyer, C. P.: A study of peroxy radicals and ozone photochemistry at coastal sites in the northern and southern hemispheres, Journal of Geophysical Research: Atmospheres, 102, 25417-25427, https://doi.org/10.1029/97JD02242, 1997.

Carpenter, L. J., Clemitshaw, K. C., Burgess, R. A., Penkett, S. A., Cape, J. N., and McFadyen, G. G.: Investigation and evaluation of the NO_x/O_3 photochemical steady state, Atmospheric Environment, 32, 3353-3365, https://doi.org/10.1016/S1352-2310(97)00416-0, 1998.

Carpenter, L. J., Fleming, Z. L., Read, K. A., Lee, J. D., Moller, S. J., Hopkins, J. R., Purvis, R. M., Lewis, A. C., Müller, K., Heinold, B., Herrmann, H., Fomba, K. W., van Pinxteren, D., Müller, C., Tegen, I., Wiedensohler, A., Müller, T., Niedermeier, N., Achterberg, E. P., Patey, M. D., Kozlova, E. A., Heimann, M., Heard, D. E., Plane, J. M. C., Mahajan, A., Oetjen, H., Ingham, T., Stone, D., Whalley, L. K., Evans, M. J., Pilling, M. J., Leigh, R. J., Monks, P. S., Karunaharan, A., Vaughan, S., Arnold, S. R., Tschritter, J., Pöhler, D., Frieß, U., Holla, R., Mendes, L. M., Lopez, H., Faria, B., Manning, A. J., and Wallace, D. W. R.: Seasonal characteristics of tropical marine boundary layer air measured at the Cape Verde Atmospheric Observatory, Journal of Atmospheric Chemistry, 67, 87-140, 10.1007/s10874-011-9206-1, 2010.

Carsey, T. P., Churchill, D. D., Farmer, M. L., Fischer, C. J., Pszenny, A. A., Ross, V. B., Saltzman, E. S., Springer-Young, M., and Bonsang, B.: Nitrogen oxides and ozone production in the North Atlantic marine boundary layer, Journal of Geophysical Research: Atmospheres, 102, 10653-10665, 10.1029/96JD03511, 1997.

Clemitshaw, K. C., Carpenter, L. J., Penkett, S. A., and Jenkin, M. E.: A calibrated peroxy radical chemical amplifier for ground-based tropospheric measurements, Journal of Geophysical Research: Atmospheres, 102, 25405-25416, https://doi.org/10.1029/97JD01902, 1997.

Cox, R. A.: Ozone and peroxy radical budgets in the marine boundary layer: Modeling the effect of NO_x, Journal of Geophysical Research: Atmospheres, 104, 8047-8056, https://doi.org/10.1029/1998JD100104, 1999.

Crawford, J., Davis, D., Chen, G., Bradshaw, J., Sandholm, S., Gregory, G., Sachse, G., Anderson, B., Collins, J., Blake, D., Singh, H., Heikes, B., Talbot, R., and Rodriguez, J.: Photostationary state analysis of the NO_2-NO system based on airborne observations from

the western and central North Pacific, Journal of Geophysical Research: Atmospheres, 101, 2053-2072, https://doi.org/10.1029/95JD02201, 1996.

Duncianu, M., Lahib, A., Tomas, A., Stevens, P. S., and Dusanter, S.: Characterization of a chemical amplifier for peroxy radical measurements in the atmosphere, Atmospheric Environment, 222, 117106, https://doi.org/10.1016/j.atmosenv.2019.117106, 2020.

Emmerson, K. M., Carslaw, N., Carslaw, D. C., Lee, J. D., McFiggans, G., Bloss, W. J., Gravestock, T., Heard, D. E., Hopkins, J., Ingham, T., Pilling, M. J., Smith, S. C., Jacob, M., and Monks, P. S.: Free radical modelling studies during the UK TORCH Campaign in Summer 2003, Atmos. Chem. Phys., 7, 167-181, 10.5194/acp-7-167-2007, 2007.

Fairlie, T. D., Jacob, D. J., Dibb, J. E., Alexander, B., Avery, M. A., van Donkelaar, A., and Zhang, L.: Impact of mineral dust on nitrate, sulfate, and ozone in transpacific Asian pollution plumes, Atmos. Chem. Phys., 10, 3999-4012, 10.5194/acp-10-3999-2010, 2010.

Gao, R. S., Keim, E. R., Woodbridge, E. L., Ciciora, S. J., Proffitt, M. H., Thompson, T. L., Mclaughlin, R. J., and Fahey, D. W.: New photolysis system for NO_2 measurements in the lower stratosphere, Journal of Geophysical Research: Atmospheres, 99, 20673-20681, https://doi.org/10.1029/94JD01521, 1994.

Handisides, G. M., Plass-Dülmer, C., Gilge, S., Bingemer, H., and Berresheim, H.: Hohenpeissenberg Photochemical Experiment (HOPE 2000): Measurements and photostationary state calculations of OH and peroxy radicals, Atmos. Chem. Phys., 3, 1565-1588, 10.5194/acp-3-1565-2003, 2003.

Hauglustaine, D. A., Madronich, S., Ridley, B. A., Walega, J. G., Cantrell, C. A., Shetter, R. E., and Hübler, G.: Observed and model-calculated photostationary state at Mauna Loa Observatory during MLOPEX 2, Journal of Geophysical Research: Atmospheres, 101, 14681-14696, https://doi.org/10.1029/95JD03612, 1996.

Hauglustaine, D. A., Madronich, S., Ridley, B. A., Flocke, S. J., Cantrell, C. A., Eisele, F. L., Shetter, R. E., Tanner, D. J., Ginoux, P., and Atlas, E. L.: Photochemistry and budget of ozone during the Mauna Loa Observatory Photochemistry Experiment (MLOPEX 2), Journal of Geophysical Research: Atmospheres, 104, 30275-30307, https://doi.org/10.1029/1999JD900441, 1999.

Hernández, M. D. A., Burkert, J., Reichert, L., Stöbener, D., Meyer-Arnek, J., Burrows, J. P., Dickerson, R. R., and Doddridge, B. G.: Marine boundary layer peroxy radical chemistry during the AEROSOLS99 campaign: Measurements and analysis, Journal of Geophysical Research: Atmospheres, 106, 20833-20846, https://doi.org/10.1029/2001JD900113, 2001.

Hosaynali Beygi, Z., Fischer, H., Harder, H. D., Martinez, M., Sander, R., Williams, J., Brookes, D. M., Monks, P. S., and Lelieveld, J.: Oxidation photochemistry in the Southern Atlantic boundary layer: unexpected deviations of photochemical steady state, Atmos. Chem. Phys., 11, 8497-8513, 10.5194/acp-11-8497-2011, 2011.

Inamdar, S., Tinel, L., Chance, R., Carpenter, L. J., Sabu, P., Chacko, R., Tripathy, S. C., Kerkar, A. U., Sinha, A. K., Bhaskar, P. V., Sarkar, A., Roy, R., Sherwen, T., Cuevas, C., Saiz-Lopez, A., Ram, K., and Mahajan, A. S.: Estimation of reactive inorganic iodine fluxes in the Indian and Southern Ocean marine boundary layer, Atmos. Chem. Phys., 20, 12093-12114, 10.5194/acp-20-12093-2020, 2020.

Jacob, D. J., Heikes, E. G., Fan, S.-M., Logan, J. A., Mauzerall, D. L., Bradshaw, J. D., Singh, H. B., Gregory, G. L., Talbot, R. W., Blake, D. R., and Sachse, G. W.: Origin of ozone and NOx in the tropical troposphere: A photochemical analysis of aircraft observations over the South Atlantic basin, 101, 24235-24250, doi:10.1029/96JD00336, 1996.

Jenkin, M. E., Young, J. C., and Rickard, A. R.: The MCM v3.3.1 degradation scheme for isoprene, Atmos. Chem. Phys., 15, 11433-11459, 10.5194/acp-15-11433-2015, 2015.

Kleindienst, T. E.: Recent developments in the chemistry and biology of peroxyacetyl nitrate, Research on Chemical Intermediates, 20, 335-384, 10.1163/156856794X00379, 1994.

Lee, J. D., Moller, S. J., Read, K. A., Lewis, A. C., Mendes, L., and Carpenter, L. J.: Year-round measurements of nitrogen oxides and ozone in the tropical North Atlantic marine boundary layer, Journal of Geophysical Research: Atmospheres, 114, https://doi.org/10.1029/2009JD011878, 2009.

Leighton, P. A.: Photochemistry of Air Pollution, Academic Press, 1961.

Liu, Y., and Zhang, J.: Atmospheric Peroxy Radical Measurements Using Dual-Channel Chemical Amplification Cavity Ringdown Spectroscopy, Analytical chemistry, 86, 5391-5398, 10.1021/ac5004689, 2014.

Ma, Y., Lu, K., Chou, C. C. K., Li, X., and Zhang, Y.: Strong deviations from the NO-NO_2-O_3 photostationary state in the Pearl River Delta: Indications of active peroxy radical and chlorine radical chemistry, Atmospheric Environment, 163, 22-34, https://doi.org/10.1016/j.atmosenv.2017.05.012, 2017.

Mahajan, A. S., Plane, J. M. C., Oetjen, H., Mendes, L., Saunders, R. W., Saiz-Lopez, A., Jones, C. E., Carpenter, L. J., and McFiggans, G. B.: Measurement and modelling of tropospheric reactive halogen species over the tropical Atlantic Ocean, Atmos. Chem. Phys., 10, 4611-4624, 10.5194/acp-10-4611-2010, 2010.

Mahajan, A. S., Whalley, L. K., Kozlova, E., Oetjen, H., Mendez, L., Furneaux, K. L., Goddard, A., Heard, D. E., Plane, J. M. C., and Saiz-Lopez, A.: DOAS observations of formaldehyde and its impact on the HO_x balance in the tropical Atlantic marine boundary layer, Journal of Atmospheric Chemistry, 66, 167, 10.1007/s10874-011-9200-7, 2011.

Mannschreck, K., Gilge, S., Plass-Duelmer, C., Fricke, W., and Berresheim, H.: Assessment of the applicability of NO-NO_2-O_3 photostationary state to long-term measurements at the Hohenpeissenberg GAW Station, Germany, Atmos. Chem. Phys., 4, 1265-1277, 10.5194/acp-4-1265-2004, 2004.

Mihele, C. M., and Hastie, D. R.: The sensitivity of the radical amplifier to ambient water vapour, Geophysical Research Letters, 25, 1911-1913, https://doi.org/10.1029/98GL01432, 1998.

Miyazaki, K., Parker, A. E., Fittschen, C., Monks, P. S., and Kajii, Y.: A new technique for the selective measurement of atmospheric peroxy radical concentrations of HO_2 and RO_2 using a denuding method, Atmos. Meas. Tech., 3, 1547-1554, 10.5194/amt-3-1547-2010, 2010.

Parrish, D. D., Trainer, M., Williams, E. J., Fahey, D. W., Hübler, G., Eubank, C. S., Liu, S. C., Murphy, P. C., Albritton, D. L., and Fehsenfeld, F. C.: Measurements of the NO_x-O_3 photostationary state at Niwot Ridge, Colorado, Journal of Geophysical Research: Atmospheres, 91, 5361-5370, https://doi.org/10.1029/JD091iD05p05361, 1986.

Parrish, D. D., Hahn, C. H., Fahey, D. W., Williams, E. J., Bollinger, M. J., Hübler, G., Buhr, M. P., Murphy, P. C., Trainer, M., Hsie, E. Y., Liu, S. C., and Fehsenfeld, F. C.: Systematic variations in the concentration of NO_x (NO + NO_2) at Niwot Ridge, Colorado, Journal of Geophysical Research: Atmospheres, 95, 1817-1836, https://doi.org/10.1029/JD095iD02p01817, 1990.

Peterson, M. C., and Honrath, R. E.: NO_x and NO_y over the northwestern North Atlantic: Measurements and measurement accuracy, Journal of Geophysical Research: Atmospheres, 104, 11695-11707, 1999.

Pinto, J. P., Dibb, J., Lee, B. H., Rappenglück, B., Wood, E. C., Levy, M., Zhang, R.-Y., Lefer, B., Ren, X.-R., Stutz, J., Tsai, C., Ackermann, L., Golovko, J., Herndon, S. C., Oakes, M., Meng, Q.-Y., Munger, J. W., Zahniser, M., and Zheng, J.: Intercomparison of field measurements of nitrous acid (HONO) during the SHARP campaign, Journal of Geophysical Research: Atmospheres, 119, 5583-5601, https://doi.org/10.1002/2013JD020287, 2014.

Pollack, I. B., Lerner, B. M., and Ryerson, T. B.: Evaluation of ultraviolet light-emitting diodes for detection of atmospheric NO_2 by photolysis - chemiluminescence, Journal of Atmospheric Chemistry, 65, 111-125, 10.1007/s10874-011-9184-3, 2010.

Prados-Roman, C., Cuevas, C. A., Hay, T., Fernandez, R. P., Mahajan, A. S., Royer, S. J., Galí, M., Simó, R., Dachs, J., Großmann, K., Kinnison, D. E., Lamarque, J. F., and Saiz-Lopez, A.: Iodine oxide in the global marine boundary layer, Atmos. Chem. Phys., 15, 583-593, 10.5194/acp-15-583-2015, 2015.

Read, K. A., Mahajan, A. S., Carpenter, L. J., Evans, M. J., Faria, B. V. E., Heard, D. E., Hopkins, J. R., Lee, J. D., Moller, S. J., Lewis, A. C., Mendes, L., McQuaid, J. B., Oetjen, H., Saiz-Lopez, A., Pilling, M. J., and Plane, J. M. C.: Extensive halogen-mediated ozone destruction over the tropical Atlantic Ocean, Nature, 453, 1232, 10.1038/nature07035 https://www.nature.com/articles/nature07035#supplementary-information, 2008.

Read, K. A., Lee, J. D., Lewis, A. C., Moller, S. J., Mendes, L., and Carpenter, L. J.: Intra-annual cycles of NMVOC in the tropical marine boundary layer and their use for interpreting seasonal variability in CO, Journal of Geophysical Research: Atmospheres, 114, https://doi.org/10.1029/2009JD011879, 2009.

Reed, C., Evans, M. J., Carlo, P. D., Lee, J. D., and Carpenter, L. J.: Interferences in photolytic NO_2 measurements: explanation for an apparent missing oxidant?, Atmospheric Chemistry Physics, 16, 4707-4724, 2016.

Reed, C., Evans, M. J., Crilley, L. R., Bloss, W. J., Sherwen, T., Read, K. A., Lee, J. D., and Carpenter, L. J.: Evidence for renoxification in the tropical marine boundary layer, Atmos. Chem. Phys., 17, 4081-4092, 10.5194/acp-17-4081-2017, 2017.

Rhoads, K. P., Kelley, P., Dickerson, R. R., Carsey, T. P., Farmer, M., Savoie, D. L., and Prospero, J. M.: Composition of the troposphere over the Indian Ocean during the monsoonal transition, Journal of Geophysical Research: Atmospheres, 102, 18981-18995, 10.1029/97JD01078, 1997.

Ridley, B. A., Carroll, M. A., Gregory, G. L., and Sachse, G. W.: NO and NO_2 in the troposphere: Technique and measurements in regions of a folded tropopause, Journal of Geophysical Research: Atmospheres, 93, 15813-15830, https://doi.org/10.1029/JD093iD12p15813, 1988.

Ridley, B. A., Madronich, S., Chatfield, R. B., Walega, J. G., Shetter, R. E., Carroll, M. A., and Montzka, D. D.: Measurements and model simulations of the photostationary state during the Mauna Loa Observatory Photochemistry Experiment: Implications for radical concentrations and ozone production and loss rates, Journal of Geophysical Research: Atmospheres, 97, 10375-10388, https://doi.org/10.1029/91JD02287, 1992.

Ryerson, T. B., Williams, E. J., and Fehsenfeld, F. C.: An efficient photolysis system for fast-response NO_2 measurements, Journal of Geophysical Research: Atmospheres, 105, 26447-26461, 10.1029/2000jd900389, 2000.

Sadanaga, Y., Matsumoto, J., Sakurai, K.-i., Isozaki, R., Kato, S., Nomaguchi, T., Bandow, H., and Kajii, Y.: Development of a measurement system of peroxy radicals using a chemical amplification/laser-induced fluorescence technique, Review of Scientific Instruments, 75, 864-872, 10.1063/1.1666985, 2004.

Saiz-Lopez, A., Plane, J. M. C., Baker, A. R., Carpenter, L. J., von Glasow, R., Gómez Martín, J. C., McFiggans, G., and Saunders, R. W.: Atmospheric Chemistry of Iodine, Chemical Reviews, 112, 1773-1804, 10.1021/cr200029u, 2012.

Sherwen, T., Evans, M. J., Carpenter, L. J., Andrews, S. J., Lidster, R. T., Dix, B., Koenig, T. K., Sinreich, R., Ortega, I., Volkamer, R., Saiz-Lopez, A., Prados-Roman, C., Mahajan, A. S., and Ordóñez, C.: Iodine's impact on tropospheric oxidants: a global model study in GEOS-Chem, Atmos. Chem. Phys., 16, 1161-1186, 10.5194/acp-16-1161-2016, 2016.

Sillman, S.: The relation between ozone, NO_x and hydrocarbons in urban and polluted rural environments, Atmospheric Environment, 33, 1821-1845, https://doi.org/10.1016/S1352-2310(98)00345-8, 1999.

Sommariva, R., Cox, S., Martin, C., Borońska, K., Young, J., Jimack, P. K., Pilling, M. J., Matthaios, V. N., Nelson, B. S., Newland, M. J., Panagi, M., Bloss, W. J., Monks, P. S., and Rickard, A. R.: AtChem (version 1), an open-source box model for the Master Chemical Mechanism, Geosci. Model Dev., 13, 169-183, 10.5194/gmd-13-169-2020, 2020.

Steinbrecher, R.: SYSTEM AND PERFORMANCE AUDIT FOR NON METHANE VOLATILE ORGANIC COMPOUNDS: Global GAW Station – Cape Verde Atmospheric Observatory Calhau, Cape Verde, WMO World Calibration Centre for VOC, Karlsruhe Institute of Technology, KIT/IMK-IFU, Garmisch-Partenkirchen, Germany, 2019.

Syomin, D. A., and Finlayson-Pitts, B. J.: HONO decomposition on borosilicate glass surfaces: implications for environmental chamber studies and field experiments, Physical Chemistry Chemical Physics, 5, 5236-5242, 10.1039/B309851F, 2003.

Tadic, I., Crowley, J. N., Dienhart, D., Eger, P., Harder, H., Hottmann, B., Martinez, M., Parchatka, U., Paris, J. D., Pozzer, A., Rohloff, R., Schuladen, J., Shenolikar, J., Tauer, S., Lelieveld, J., and Fischer, H.: Net ozone production and its relationship to nitrogen oxides and volatile organic compounds in the marine boundary layer around the Arabian Peninsula, Atmos. Chem. Phys., 20, 6769-6787, 10.5194/acp-20-6769-2020, 2020.

Trebs, I., Mayol-Bracero, O. L., Pauliquevis, T., Kuhn, U., Sander, R., Ganzeveld, L., Meixner, F. X., Kesselmeier, J., Artaxo, P., and Andreae, M. O.: Impact of the Manaus urban plume on trace gas mixing ratios near the surface in the Amazon Basin: Implications for the NO-NO_2-O_3 photostationary state and peroxy radical levels, Journal of Geophysical Research: Atmospheres, 117, https://doi.org/10.1029/2011JD016386, 2012.

Vaughan, S., Ingham, T., Whalley, L. K., Stone, D., Evans, M. J., Read, K. A., Lee, J. D., Moller, S. J., Carpenter, L. J., Lewis, A. C., Fleming, Z. L., and Heard, D. E.: Seasonal observations of OH and HO_2 in the remote tropical marine boundary layer, Atmos. Chem. Phys., 12, 2149-2172, 10.5194/acp-12-2149-2012, 2012.

Vogt, R., Sander, R., von Glasow, R., and Crutzen, P. J.: Iodine Chemistry and its Role in Halogen Activation and Ozone Loss in the Marine Boundary Layer: A Model Study, Journal of Atmospheric Chemistry, 32, 375-395, 10.1023/A:1006179901037, 1999.

Volz-Thomas, A., Pätz, H.-W., Houben, N., Konrad, S., Mihelcic, D., Klüpfel, T., and Perner, D.: Inorganic trace gases and peroxy radicals during BERLIOZ at Pabstthum: An investigation of the photostationary state of NO_x and O_3, Journal of Geophysical Research: Atmospheres, 108, PHO 4-1-PHO 4-15, https://doi.org/10.1029/2001JD001255, 2003.

Wang, X., Jacob, D. J., Downs, W., Zhai, S., Zhu, L., Shah, V., Holmes, C. D., Sherwen, T., Alexander, B., Evans, M. J., Eastham, S. D., Neuman, J. A., Veres, P. R., Koenig, T. K., Volkamer, R., Huey, L. G., Bannan, T. J., Percival, C. J., Lee, B. H., and Thornton, J. A.: Global tropospheric halogen (Cl, Br, I) chemistry and its impact on oxidants, Atmos. Chem. Phys., 21, 13973-13996, 10.5194/acp-21-13973-2021, 2021.

Whalley, L. K., Lewis, A. C., McQuaid, J. B., Purvis, R. M., Lee, J. D., Stemmler, K., Zellweger, C., and Ridgeon, P.: Two high-speed, portable GC systems designed for the measurement of non-methane hydrocarbons and PAN: Results from the Jungfraujoch High Altitude Observatory, Journal of Environmental Monitoring, 6, 234-241, 10.1039/B310022G, 2004.

Whalley, L. K., Furneaux, K. L., Goddard, A., Lee, J. D., Mahajan, A., Oetjen, H., Read, K. A., Kaaden, N., Carpenter, L. J., Lewis, A. C., Plane, J. M. C., Saltzman, E. S., Wiedensohler, A., and Heard, D. E.: The chemistry of OH and HO_2 radicals in the

boundary layer over the tropical Atlantic Ocean, Atmos. Chem. Phys., 10, 1555-1576, 10.5194/acp-10-1555-2010, 2010.

Williams, E. J., Roberts, J. M., Baumann, K., Bertman, S. B., Buhr, S., Norton, R. B., and Fehsenfeld, F. C.: Variations in NO_y composition at Idaho Hill, Colorado, Journal of Geophysical Research: Atmospheres, 102, 6297-6314, https://doi.org/10.1029/96JD03252, 1997.

Wofsy, S. C., Afshar, S., Allen, H. M., Apel, E. C., Asher, E. C., Barletta, B., Bent, J., Bian, H., Biggs, B. C., Blake, D. R., Blake, N., Bourgeois, I., Brock, C. A., Brune, W. H., Budney, J. W., Bui, T. P., Butler, A., Campuzano-Jost, P., Chang, C. S., Chin, M., Commane, R., Correa, G., Crounse, J. D., Cullis, P. D., Daube, B. C., Day, D. A., Dean-Day, J. M., Dibb, J. E., DiGangi, J. P., Diskin, G. S., Dollner, M., Elkins, J. W., Erdesz, F., Fiore, A. M., Flynn, C. M., Froyd, K. D., Gesler, D. W., Hall, S. R., Hanisco, T. F., Hannun, R. A., Hills, A. J., Hintsa, E. J., Hoffman, A., Hornbrook, R. S., Huey, L. G., Hughes, S., Jimenez, J. L., Johnson, B. J., Katich, J. M., Keeling, R. F., Kim, M. J., Kupc, A., Lait, L. R., McKain, K., McLaughlin, R. J., Meinardi, S., Miller, D. O., Montzka, S. A., Moore, F. L., Morgan, E. J., Murphy, D. M., Murray, L. T., Nault, B. A., Neuman, J. A., Newman, P. A., Nicely, J. M., Pan, X., Paplawsky, W., Peischl, J., Prather, M. J., Price, D. J., Ray, E. A., Reeves, J. M., Richardson, M., Rollins, A. W., Rosenlof, K. H., Ryerson, T. B., Scheuer, E., Schill, G. P., Schroder, J. C., Schwarz, J. P., St.Clair, J. M., Steenrod, S. D., Stephens, B. B., Strode, S. A., Sweeney, C., Tanner, D., Teng, A. P., Thames, A. B., Thompson, C. R., Ullmann, K., Veres, P. R., Wagner, N. L., Watt, A., Weber, R., Weinzierl, B. B., Wennberg, P. O., Williamson, C. J., Wilson, J. C., Wolfe, G. M., Woods, C. T., Zeng, L. H., and Vieznor, N.: ATom: Merged Atmospheric Chemistry, Trace Gases, and Aerosols, Version 2, in, ORNL Distributed Active Archive Center, 2021.

Wolfe, G. M., Cantrell, C., Kim, S., Mauldin Iii, R. L., Karl, T., Harley, P., Turnipseed, A., Zheng, W., Flocke, F., Apel, E. C., Hornbrook, R. S., Hall, S. R., Ullmann, K., Henry, S. B., DiGangi, J. P., Boyle, E. S., Kaser, L., Schnitzhofer, R., Hansel, A., Graus, M., Nakashima, Y., Kajii, Y., Guenther, A., and Keutsch, F. N.: Missing peroxy radical sources within a summertime ponderosa pine forest, Atmos. Chem. Phys., 14, 4715-4732, 10.5194/acp-14-4715-2014, 2014.

Wood, E. C., and Charest, J. R.: Chemical Amplification - Cavity Attenuated Phase Shift Spectroscopy Measurements of Atmospheric Peroxy Radicals, Analytical chemistry, 86, 10266-10273, 10.1021/ac502451m, 2014.

Yang, M., Beale, R., Liss, P., Johnson, M., Blomquist, B., and Nightingale, P.: Air–sea fluxes of oxygenated volatile organic compounds across the Atlantic Ocean, Atmos. Chem. Phys., 14, 7499-7517, 10.5194/acp-14-7499-2014, 2014.

Zellweger, C., Steinbacher, M., and Buchmann, B.: Evaluation of new laser spectrometer techniques for in-situ carbon monoxide measurements, Atmos. Meas. Tech., 5, 2555-2567, 10.5194/amt-5-2555-2012, 2012.

Zellweger, C., Emmenegger, L., Firdaus, M., Hatakka, J., Heimann, M., Kozlova, E., Spain, T. G., Steinbacher, M., van der Schoot, M. V., and Buchmann, B.: Assessment of recent advances in measurement techniques for atmospheric carbon dioxide and methane observations, Atmos. Meas. Tech., 9, 4737-4757, 10.5194/amt-9-4737-2016, 2016.